This manuscript has been peer-reviewed and accepted for publication in **AGU Books: Extensional Tectonics: Continental Breakup to Formation of Oceanic Basins**. Shortly, the "Peer-reviewed publication DOI" link will be updated on this preprint server. We hope you find this paper interesting and would welcome your feedback on it.

Kindly contact Folarin Kolawole (*fola@ldeo.columbia.edu*) with any feedback that you may have.

Rapid Versus Delayed Linkage and Coalescence of Propagating Rift Tips

Folarin Kolawole[1]*, Liang Xue[2], Zuze Dulanya[3]

[1]Department of Earth and Environmental Sciences, Lamont-Doherty Earth Observatory of Columbia University, New York, USA
[2]Department of Earth and Environmental Sciences, Syracuse University, Syracuse, NY, USA
[3]Geography and Earth Sciences Department, University of Malawi, Zomba, Malawi

Correspondence to: F. Kolawole (fola@ldeo.columbia.edu)

Abstract

The tectonic interaction, linkage, and coalescence of propagating continental rift segments eventually create a through-going axial rift floor without which a break-up axis cannot develop. However, prior to linkage, interacting rifts are separated by a topographic basement-high (rift interaction zone, RIZ) which is progressively dismembered and down-thrown by the lateral propagation of rift-tip faulting and their hanging wall subsidence. Here, we explore the evolution of the Middle Shire and Nsanje RIZs located along three contiguous non-volcanic propagating rift segments: the southern Malawi Rift (SMR), Lower Shire Graben (LSG), and the Nsanje Graben (NG), East Africa. The Middle Shire RIZ is an overlapping-oblique divergent RIZ in which the NNE/N-trending SMR is propagating southwards into the shoulder of the NW-trending LSG, whereas the Nsanje RIZ is a tip-to-tip oblique RIZ in which the LSG has propagated southeast into the northern tip of the N-trending NG. We utilize field observations and a landscape evolution model with implemented fault displacement fields of two contiguous RIZs with contrasting geometries, to simulate their geomorphic evolution, and apply a static stress model to evaluate the stress transfer patterns during RIZ evolution. The model results provide insights into the natural observations in the study area, in which, with progressive extension and tip growth, the Middle Shire RIZ maintains minor basement down-throw and an unequilibrated axial stream profile, which contrasts the widespread basement burial and equilibrated axial stream profile across the Nsanje RIZ. Modeled static stress distribution predicts compounding stress concentrations at tip-to-tip RIZs (synthetic border fault interactions), favoring brittle strain localization and rift coalescence, and stress relaxation at overlapping divergent RIZs (antithetic border fault interactions), favoring stalled rift coalescence. We argue that RIZ and rift border fault geometries, and their kinematics strongly influence the pace of rift coalescence by modulating the spatial distribution of tectonic stresses necessary to promote rift-linking deformation.

Keywords: Continental Rift, Rift Linkage, Rift Interaction Zone, Landscape Evolution

1. Introduction

In continental lithosphere, the initiation of a divergent plate boundary is manifested by the development of a system of isolated graben and half-graben rift basins, each representing a rift segment (Figure 1a; e.g., Rosendahl et al., 1986; Rosendahl 1987; Ebinger et al., 1987; Corti et al., 2007; Nelson et al., 1992; Kolawole et al., 2021a). Some rift segments may nucleate as a system of sub-basins with early establishment of the length of the entire border fault system (Rotevatn et al., 2018), whereas others nucleate by a progressive lateral growth of the border fault (Agar and Klitgord, 1995). In narrow continental rift systems, although nucleating rift border faults may initially terminate at mis-oriented pre-rift basement shear zones or strong crustal blocks, stress build-up and magmatism at rift tips may drive renewed propagation of the rift basin (Ebinger et al., 1989; van Wijk and Blackman, 2005; Kolawole et al., 2022). With continued tectonic extension of the lithosphere, which may occur over multiple rift phases, rift basins deepen and lengthen by means of the three-dimensional propagation of their basin-bounding and intrabasinal fault systems, during which tectonic strain may migrate between the faults and sub-basins (e.g., Ebinger et al., 1989, 2000; Heilman et al; 2019; Fazlikhani et al., 2021; Scholz et al., 2020; Kolawole et al., 2022; Shaban et al., 2023). However, the inherited crustal rheology may temporarily stagnate the lateral propagation of a rift tip (e.g., van Wijk and Blackman, 2005; Kolawole et al., 2022; Shaban et al., 2023), during which mantle flow patterns beneath the rift tip promote stress build-up and shear zone formation (e.g., van Wijk and Blackman, 2005). As propagating rift tips encroach into unrifted basement areas in the intervening region between the rift segments, their faults may interact and transfer tectonic strain, leading to the hard- and/or soft-linkage of the faults (Figures 1b-c; McClay and Khalil, 1998; McClay et al., 2002; Fossen and Rotevatn, 2016; Kolawole et al., 2021a). These intervening regions of unrifted basement are usually of large spatial scales (~100 – 200-km length scales) and are referred to as Rift Interaction Zones (RIZ in Figures 1a-c; Nelson et al., 1992; Koehn et al., 2008; Aanyu and Koehn, 2011; Sachau et al., 2015; Kolawole et al., 2021a). It is within this broad RIZ region that relatively smaller-scale (~50 km length scale) deformation and strain transfer features such as 'Transfer Zones' and 'Accommodation Zones' develop to facilitate rift linkage (Figures 1a-b; Bosworth, 1985; Ebinger et al., 1987; Coffield and Schamel, 1989; Morley et al., 1990; Morley, 1995; Faulds and Varga, 1998; Withjack et al., 2002).

Eventually, the linkage of the propagating rift segments is succeeded by the coalescence of the rift basins, forming a composite rift basin with a through-going rift floor of pronounced crustal subsidence and significant basement burial along a localized narrow rift system (Figure 1c). RIZs constitute 'sticky crustal blocks', and the significance of rift segment coalescence is founded on the grounds that a successful through-going break-up axis cannot develop along an evolving continental rift system without the structural breaching of its RIZs. During the process of rift linkage, a deforming RIZ transitions from an unbreached RIZ, to partially breached, and breached RIZ; where an additional stage of 'recently breached' RIZ is observable in modern active continental rift systems (Kolawole et al., 2021a). Also, the maximum length of a rift border fault is determined by the effective elastic thickness of the lithosphere (Ebinger et al., 1999), such that after the coalescence of isolated rift basins, the resulting composite rift basin is made up of multiple border fault systems that flip polarity along-strike (e.g., Bosworth, 1985; Rosendahl et al., 1986; Ebinger et al., 1987; Rosendahl, 1987; Sander and Rosendahl, 1989; Patton et al., 1994; Lao-Davila et al., 2016; Heilman et al., 2019). Segmentation zones of extensional systems also play important roles during the mature stages of divergent plate boundary development. For example, during continental break-up, delayed propagation of the break-up axis

(oceanic ridge tip) promotes excess magmatism at the segmentation zones where the ridge propagation is stalled (Koopmann et al., 2014).

Analog and numerical modeling experiments of rift linkage, mostly focused on underlapping and overlapping parallel rift segments, show that various kinematics of faulting may develop in the zone of rift interaction, with geometrical and mechanical controls of inherited basement structure (e.g., Wilson, 1990; Acocella et al., 1999; Corti, 2004; Aanyu and Koehn, 2011; Corti, 2012; Neuharth et al., 2021; Wolf et al., 2022). Indeed, a few recently published models incorporated obliquely oriented rifts (Molnar et al., 2019; Schmid et al., 2023). However, natural rift systems exhibit a broader variety of three-dimensional RIZ geometries which include tip-to-tip, oblique, and orthogonal plan-view geometries for rift pairs in which the rift border faults, although separated by up to 300 km, may have synthetic dip polarity defining a 'convergent' geometry or are antithetic to one another representing a 'divergent' geometry (Kolawole et al., 2021a). Although RIZs are larger-scale structures than Transfer Zones, the convention of 'convergent' and 'divergent' terminology to describe the 3-D structure of RIZs is adopted from the Transfer Zone classification of Morley et al. (1990). The complexity of RIZ geometries also encompasses triple and quadruple junctions that feature three or more juvenile rift segments (Kolawole et al., 2021a). Some of the enigmatic RIZ geometries are the overlapping divergent RIZs in which the rifts are oriented obliquely or orthogonally to one another, such that the border faults of a rift segment are propagating into the uplifting footwall of the border faults (or rift flank) of the other rift basin. The diverse RIZ geometries demonstrate a greater three-dimensional complexity than the simple parallel and overlapping geometries commonly adopted in many published numerical and analog modeling studies of rift segment interaction.

In this contribution, we investigate the potential tectonic factors that may promote, inhibit, or delay the pace of rift linkage and coalescence, and test the hypothesis that RIZ geometry and the associated kinematics may constitute one of these factors. We explore the structure, fault kinematics, displacement and stress transfer fields, and landscape evolution of two RIZs separating three contiguous actively propagating magma-poor rift segments in the southern East African Rift System: the southern Malawi Rift, Lower Shire Graben, and the Nsanje Graben (Figure 2). The Middle Shire RIZ is an overlapping oblique divergent RIZ in which the NNE/N-trending southern Malawi Rift is propagating southwards into the NE shoulder of the NW-trending Lower Shire Graben, whereas the Nsanje RIZ is a tip-to-tip oblique RIZ (convergent) in which the Lower Shire Graben has propagated southeast into the northern tip of the N-trending Nsanje Graben. The two RIZs provide natural examples to explore strain localization on rift tips and RIZ syn-rift evolution in the absence of magmatism. We utilize field observations, landscape evolution, and static stress distribution models to examine the potential influence of the contrasting RIZ geometries on the long-term evolution of the RIZs.

1.1. The Zomba - Lower Shire - Nsanje Rift Zone

1.1.1. Pre-Rift Basement Geology

The east African basement is characterized by Archean and Paleoproterozoic cratonic blocks that are surrounded by Meso- to Neoproterozoic orogenic belts (Fritz et al., 2013). The orogenic belts are composed of exhumed igneous and metamorphic rocks of mostly amphibolite to granulite facies

grades, with sporadic occurrences of eclogite facies rocks that are localized along ductile terrane boundary shear zones (e.g., Daly et al., 1991; Fritz et al., 2013). These orogenic belts developed during multiple Meso- to Neoproterozoic orogenic events that witnessed the amalgamation of Gondwana (Fritz et al., 2013). In the Phanerozoic, East Africa has experienced repeated phases of tectonic extension, in which the rift systems follow the mobile belts and avoid the cratonic blocks (Daly et al., 1989; Corti et al., 2007).

The southern Malawi Rift and Shire Rift Zone developed along tectonic boundaries that separate distinct Precambrian orogenic belts or terranes. These include the Southern Irumide Belt (1060 - 950 Ma), Zambezi Belt (1830 - 795 Ma), the Tete-Chipata Complex, and the Unango Complex (1060 - 950 Ma) (Barr and Brown, 1987; Hargrove et al 2003; Fritz et al., 2013) (Figure S1), whereas the Nsanje Graben developed within the Nampula Complex (1025-1075 Ma). The basement terranes along these mobile belts are composed of Mesoproterozoic crust which has been reworked and overprinted by contractional structures and igneous intrusions of the Neoproterozoic Pan African Orogeny. Common rock types found in the mobile belts include schists, amphibolite and granulitic gneisses, deformed granites, granodiorites, syenites, gabbro, and anorthosites (e.g., Barr and Brown, 1987; Fritz et al., 2013).

1.1.2. Rift Structure and Tectonic History

The Phanerozoic Eon of eastern Africa has witnessed three distinct phases of tectonic extension that localized rift basins along the Precambrian mobile belts (Delvaux, 1989; Castaing, 1991; Chorowicz, 2005). The first rifting phase occurred in the Permian – Early Jurassic, known as the 'Karoo' event, the second event occurred in the Late Jurassic - Cretaceous, and the third event is the current phase of tectonic extension known as the 'East African Rift System' (EARS; Delvaux, 1989; Castaing, 1991). The rift system is characterized by a network of rift segments that define multiple branches, mainly the Eastern, Western, Southern, and Southwestern branches (Figure 2). The Eastern Branch is magma-rich manifested by widespread volcanism along the rift basins; whereas the Western, Southern, and Southwestern branches are largely magma-poor with surface volcanism restricted to four rift interaction zones (Figure 2). The Karoo and Cretaceous rift segments and associated faults were commonly reactivated in the Cenozoic rift phase (Castaing, 1991; Morley et al., 1999; Daly et al., 2020; Kolawole et al., 2018; 2021b, 2022). However, there is increasing evidence suggesting that the transition from Mesozoic to Cenozoic rifting phases was accompanied by the abandonment of some of the early-rift fault segments, sub-basins, and in some cases, entire rift segments (e.g., blue lines of 'inactive rifts' in Figure 2; Delvaux, 1989; Castaing, 1991; Ragon et al., 2019; Kolawole et al., 2022). Considering the history pronounced magmatic Karoo and Cretaceous rifting in the southern Malawi-central Mozambique region, the 'pre-rift basement' of the Cenozoic rift phase is characterized by a basal Precambrian metamorphic unit and its overlying volcano-sedimentary sequences of Mesozoic rift deposits (Castaing, 1991; Kolawole et al., 2021).

The Zomba, Lower Shire, and Nsanje grabens define a system of three contiguous active rift basins that extend between the southern Malawi and central Mozambique regions of EARS's magma-poor southern branch (Figure 2). Thermochronological modeling suggests that the border faults have been active since the Late Oligocene - Early Miocene, with a possible onset of Cenozoic rifting as early as

the Eocene (Bicca et al., 2019; Ojo et al., 2022a). Current geodetic extension rates in the region is ca. 2.2 mm/yr (Stamps et al., 2018), with a regional normal faulting stress regime of ENE-WSW-oriented minimum principal compressive stress axis, σ_3 (Williams et al., 2019) (Figure 3a). Geodetic extension rates vary along-trend of the Malawi Rift (Saria et al., 2014). Seismic- and gravity-derived estimates of crustal thickness beneath the grabens range ca. 40 - 43 km (Njinju et al., 2019; Sun et al., 2021); lithospheric thickness is ca. 130 km, but thins to ca. 110 km beneath the Shire Rift Zone (Njinju et al., 2019a). The distribution of aeromagnetic Curie Point depths suggests an elevated heat flow of ca. 76 mWm^{-2} within the grabens relative to the ca. 66 mWm^{-2} in the rift flanks (Njinju et al., 2019b).

The NNE-trending Zomba Graben is the southernmost section of the Malawi Rift and is bounded by the Zomba Fault to the east and Lisungwe and Wamkurumadzi Fault systems to the west (Figure 3a). The border faults generally follow the large-scale trends of the Precambrian metamorphic fabrics, indicating basement control on border fault localization (Williams et al., 2019; Kolawole et al., 2021a). Rift sedimentation in the Zomba Graben is primary localized in the northern, northeastern, and western parts of the graben (Figure 3b) and are dominated by unconsolidated Quaternary fluvial deposits and outcrops of clay-rich Matope paleo-lake sediments with characteristic shoreline gravels (Dulanya, 2017). The southern section of the graben is dominated by Precambrian basement exposures along the rift floor (Figure 3b; Kolawole et al., 2021a). The magnitudes of cumulative border fault offset along the Malawi Rift generally decrease southward, and the deepest syn-rift sedimentary sequences in the northern sub-basins of the rift appear to be absent in the south, suggesting an overall long-term southward propagation of the rift basin (Specht and Rosendahl, 1989; Scholz et al., 2020). South of Lake Malawi, shallow boreholes, electrical resistivity tomography, and depth-to-magnetic basement show rift sediment thickness of not more than 600 m (Bloomfield, 1965; Ojo et al., 2022b).

The NW-trending Lower Shire Graben is located south of the Zomba Graben and represents the easternmost sub-basin of the Shire Rift Zone, a multiphase rift basin in east Africa (Castaing, 1991; Kolawole et al., 2022). The Lower Shire Graben is bounded to the northeast by the Thyolo-Muona-Ruo Fault System in the east and to the southwest by the Panga Fault. The basin shows widespread coverage of Quaternary deposits (Figure 3b), with the thickest sections potentially occurring in the hanging wall of the Thyolo and Muona faults, dominated by the fluviolacustrine sequences of the Elephant Marsh and Shire River (Kolawole, 2020; Kolawole et al., 2022). The localization of the Elephant Marsh along the hanging wall of the Thyolo Fault, and the spatial correlation of the lateral changes in the geometry of the marsh with prominent changes in the Thyolo Fault displacement profile suggest structural control on the development of the wetland (Kolawole, 2020). The rift axis hosts a buried segment of a large-offset fault, the southern segment of the Mwanza Fault, which is interpreted to be the eastern border fault of the Shire Rift Zone during the Mesozoic phases of extension (Kolawole et al., 2022). Similar to the Zomba Graben, the Mwanza and the Thyolo-Muona-Ruo border fault systems of the Lower Shire Graben generally follow the large-scale trends of the Precambrian metamorphic fabrics, indicating basement control on border fault localization (Wedmore et al., 2020a; Kolawole et al., 2022). However, the southeastern tip of the Ruo Fault crosscuts the NE-trending basement fabrics of the Precambrian Lurio Shear Zone (Kolawole et al., 2022). Outcrops of Mesozoic volcano-sedimentary sequences near the SW margin of the graben, and confinement of basaltic aeromagnetic fabrics to the hanging wall of the buried Mwanza Fault segment suggest the presence of Mesozoic rift deposits beneath the Cenozoic sediments in the southwestern half of the graben (Kolawole et al., 2022). Depth-to-magnetic basement estimates suggest that the present-day

NE border fault, Thyolo-Muona-Ruo Fault system may have accrued a larger post-Mesozoic vertical displacement (ca. 1.5 km) than the the SW border fault, the Panga Fault (< 200 m) (Kolawole et al., 2022). Despite up to 3 km erosion of the early rift sediments during the Mesozoic rifting phases (Bicca et al., 2019), the present-day cumulative sediment thickness along the graben axis is estimated to be at least 2.4 km (Kolawole et al., 2022). This suggests a possible Cenozoic strain accommodation along the graben axis prior to the apparent 'abandonment' and burial of the southern Mwanza Fault.

The N-to-NNE-trending Nsanje Graben is located south of the Lower Shire Graben, and it defines the northern continuation of the Urema Graben system of Mozambique (Figure 2; Pfaffling et al., 2009). The graben is bounded to the west by the Nsanje Fault, and to the east by the Ndidi Fault (Figure 3a). Both the Nsanje and Ndindi border faults crosscut the large-scale NE-trending metamorphic fabrics of the host Precambrian basement (Bloomfield, 1958; Kolawole et al., 2022; Thomas et al., 2022), indicating a lack of large-scale basement inheritance on border fault development. Geologic maps show widespread coverage of Quaternary sediments across the entire graben, deposited in the Ndindi Marsh and floodplains of the Shire River (Figures 3b; Bloomfield, 1958; Choubert et al., 1988).

1.1.3. The Middle Shire and Nsanje Rift Interaction Zones

The Middle Shire RIZ, which represents the zone of transition from the Zomba Graben to the Lower Shire Graben, is characterized by a rotation of the Precambrian metamorphic basement fabrics from NNE-SSW trend in the Zomba Graben area to a NW-SE trend in the Lower Shire Graben (Kolawole et al., 2021a). The Nsanje RIZ, which represents the zone of transition from the Lower Shire Graben to the Nsanje Graben occurs at the NE-trending Lurio Shear Zone, an exhumed ductile shear zone separating the Unango and Nampula terranes of the Precambrian Southern Irumide Belt (Figure S1; Fritz et al., 2013; Kolawole et al., 2022; Thomas et al., 2022). The Middle Shire RIZ defines an overlapping oblique divergent RIZ geometry in which the NNE/N-trending Malawi Rift is propagating southwards into the NE shoulder of the NW-trending Lower Shire Graben, whereas the Nsanje RIZ is a tip-to-tip oblique RIZ ('convergent' border fault polarity pattern) in which the Lower Shire Graben has propagated southeast into the northern tip of the N-trending Nsanje Graben (Figure 3a).

In contrast to the Nsanje RIZ which shows very sparse surface exposures of the Precambrian basement along the modern rift floor, the Middle Shire RIZ is dominated by widespread exposures of the basement (Figures 3b, 4a-b, 4c-d). In the Middle Shire RIZ, the rift floor tilts westwards towards the escarpments of the Lisungwe and Wamkurumadzi Faults (e.g., Figure 4a). In the Nsaje RIZ, the rift floor also tilts to the southwest but there is no surface expression of faulting (Figures 3b, 4c-d, S2). Longitudinal topographic relief profile of the rift axis shows that the Zomba Graben and Middle Shire RIZ are at a higher structural elevation than the Nsanje Graben (Figure 4e). Thus, based on the criteria of border fault connectivity, cross-over topographic and axial stream morphology, and directionality of axial stream flow, the Middle Shire RIZ is interpreted to be a recently breached RIZ, and the Nsanje Graben a breached RIZ that is undergoing rift coalescence (Kolawole et al., 2021a).

1.1.4. Modern Rift Basin Drainage Geomorphology

The southern Malawi-central Mozambique region is characterized by a tropical climate, in which dry seasons generally extend from April to September (average annual rainfall of~0.65 m at Tete), and wet seasons from October to March (Garzanti et al., 2022). The modern landscape of the Zomba-Lower Shire-Nsanje graben system is drained by the Shire River and its 18,000 km^2 catchment area (Figure 3a). The south-flowing, ca. 490 km-long axial stream represents the largest river in Malawi, the only outlet for Lake Malawi, and one of the major tributaries of the Zambezi River (Price, 1966; Palamuleni et al., 2011; Dulanya, 2017). Zambezi River Delta represents one of the largest sediment supply points into the Mozambique Channel arm of the Indian Ocean, highlighting the significance of the Shire River for sediment contributions into the ocean basin depositional sink (Garzanti et al., 2022). Although the Shire River represents the only modern fluvial link between Lake Malawi and the Indian Ocean, the trunk stream is punctuated by major sediment sinks which includes Elephant Marsh in the Lower Shire Graben and Ndindi Marsh in the Nsanje Graben (Figure 3a). The Elephant Marsh and Ndindi Marsh represent wetlands that have developed in the axial depocenters of the Lower Shire and Nsanje grabens, but are connected across the Nsanje RIZ, and the transition between the two wetlands is defined by a zone of decrease in width of the wetland within the Nsanje RIZ (Figure 3b).

The river course is divided into the 'Upper Shire' section at ca. 500 m elevation in the Zomba Graben, the 'Middle Shire' section in the Middle Shire RIZ where the river drops across a ca. 80 m escarpment over 72 km distance, and the 'Lower Shire' section at ca. 45 - 50 m elevation in the Lower Shire Graben (Figure 4e). The rectilinear planform geometry, the large-scale relief morphology of the longitudinal elevation profile of the Middle Shire section, as well as the clustering of rapids and waterfalls (i.e., knickpoints) within the section (see Figure 4b) suggests that the Middle Shire section is not equilibrated with the downstream sections of the stream profile (Dulanya, 2017; Kolawole et al., 2021a; Dulanya et al., 2022). More importantly, in contrast to the axial stream profile within the Middle Shire RIZ, the 'flat' longitudinal relief morphology and sinuous planform geometry of the axial stream across the Nsanje RIZ (Figures 4d-e) suggests an equilibrated profile. These observations are also consistent with the contrasts in the axial stream planform morphology between the two RIZs, whereby in the Middle Shire RIZ, the axial stream exhibits significantly lower channel sinuosity and channel width in contrast to the Nsanje RIZ (Kolawole et al., 2021a). Furthermore, the highly sinuous axial stream planform morphology of the Lower Shire section generally continues southwards through the Nsanje RIZ and the Nsanje Graben.

Investigation of the knickpoint initiation times in the Middle Shire River catchment suggested that the Upper and Lower Shire were not integrated into a single south-flowing stream until around the Mid-Pleistocene (Dulanya et al. 2022). The Middle Shire region is interpreted to have been an elevated basement block that previously isolated the Lower Shire Graben from the Zomba Graben, at the time of which the Lower Shire River section flowed south, and the Upper Shire hosted a lake (paleo-lake Matope) that flowed north into Lake Malawi with alternating periods flooding of Lake Malawi into the Zomba Graben (Dulanya, 2017). The subsequent integration of the axial stream across the Middle Shire is likely to have been facilitated by the continued brittle deformation and down-faulting of the Middle Shire basement by the tectonic interaction between the northwestward propagation of the Thyolo Fault and possibly, a simultaneous propagation of the southern Zomba Graben faults (Kolawole et al., 2021a). Thus, the structural breaching of the Middle Shire RIZ and the linkage of the Zomba and Lower Shire grabens is inferred to have taken place as recent as the Mid Pleistocene, relative to the Oligocene-Miocene initiation of Cenozoic rifting in the region (Dulanya et al., 2022).

297

298 2. Methods

299 2.1. Field Observations as Constraints on Rift Kinematics

300 To constrain the kinematics of rifting in southern Malawi, we perform field investigations on the
301 outcrops of border faults in the Lower Shire and Nsanje grabens (locations are 'red stars' in Figure
302 3a). The natural observations of fault kinematics from the study area provide constraints on our
303 numerical model (see section 2.2). Our fieldwork involved the collection of measurements of slip
304 indicators on the slip surfaces of the border faults, which include strike and dip of fault surfaces, and
305 the trend and plunge of highest quality slip stria on the surfaces. As for the Zomba Graben, we utilize
306 published field measurements (from Wedmore et al., 2020b) taken along the largest intrabasinal fault
307 in the basin, the Chingale Step Fault. These measurements (see Table 1) allow us to estimate a single
308 kinematic strain tensor that is compatible with the kinematics of three rift basins in the current regional
309 tectonic stress field. For this analysis, we utilize the FaultKin program (Marrett and Allmendinger,
310 1990; Cladouhos and Allmendinger, 1993), adopting a uniform weight moment tensor summation.
311 The program determines the principal strain directions using slip surfaces with known geometries and
312 striae with known slip senses as input, while assuming that the deformation is coaxial. The analysis is
313 a standard technique that produces a fault plane solution with two orthogonal nodal planes, the
314 bisectors of which produce P- and T-axes of the incremental strain tensor. The P- and T-axes
315 respectively represent the principal shortening (ε_3) and principal extension (ε_1) strain axes of the array
316 of input faults.

317

318 2.2. Modeling Landscape Evolution

319 We use the Fastscape algorithm (Braun and Willett, 2013) to solve the stream power law to estimate
320 the response of surface processes to rift tip propagation in different RIZs. The Fastscape code
321 simulates bedrock river incision and deposition by (Yuan et al., 2019):

322

323 $$\frac{\partial h}{\partial t} = U - KA_m S_n + \frac{G}{A}\int_A \left(U - \frac{\partial h}{\partial t}\right) dA \quad \text{where } h \geq h_{base} \qquad (1)$$

324 $$\frac{\partial h}{\partial t} = K_b \nabla^2 h + \int_A \left(\frac{U - \partial \frac{h}{\partial} t}{\partial x \partial y}\right) dA \quad \text{where } h < h_{base} \qquad (2)$$

325

326 Where h and h_{base} is the elevation and elevation of rift lake, respectively, so Equation 1 and 2 represent
327 the landscape evolution on the land and in the rift lake, t is time, U, A, S are uplift rate, drainage area,
328 and local slope respectively. K and G reflect the lithology erodibility and deposition coefficient, K_b is
329 the diffusion coefficient in the rift lake, presumably linearly corresponding to local slope, with a value
330 of 30. m, n are poorly constrained constants that most depend on lithology and climate. We use m =
331 0.5, n =0.1, K = 4e-6, G = 1e-3 based on previous work (e.g., Croissant and Braun, 2014, Guerit et
332 al., 2019; Yuan et al., 2019).

The domain is 500 km by 500 km with cell size of 1 km^2 (Figures 5a-c). With a focus on the effects of rift segment tip propagation, we simplify the impacts of climate and lithology in the model and assume a constant rainfall of 1m/yr in the study area and a homogenous lithology. We apply the fixed value boundary condition for the four borders. The model time is 10 Myr with a timestep of 1 kyr; and we present results for the 5 Myr and 10 Myr timesteps. The model domain contains three contiguous grabens: NNE-trending Rift 1 in the north, NW-trending Rift 2 in the center, and NNE-trending Rift 3 in the south (Figure 5c). The orientation of each graben-bounding fault reflects the location of border faults in the Zomba Graben (southern Malawi Rift), Lower Shire Graben, and Nsanje Graben, thus defining an oblique overlapping divergent RIZ between rifts 1 and 2, and an underlapping oblique convergent RIZ between rifts 2 and 3 (Figure 5c). Based on field observations along the major faults of the Zomba - Lower Shire - Nsanje graben system (see section 3.1; Figures 6a-h), we impose a normal faulting tectonic stress regime on each border fault in the model, such that each model rift basin undergoes orthogonal extension. The displacement of graben-bounding (border) normal faults is added as time-dependent uplift fields on topography. The maximum displacement, posted at the center of each fault, is 0.8 mm/yr and it decreases to zero at the tips of the faults, following a sinusoidal curve. The half-extension rate and tip growth rate are 1 mm/yr and 5 mm/yr, respectively for all border faults in the study area (Figure 4), based on the observed low extension rate of 2.2 mm/yr (Stamps et al., 2018). Positive displacement indicates uplift and negative displacement indicates subsidence; the background displacement rate in the model is 0.03 mm/yr (Figures 5a-b). In the model, each rift propagates bi-directionally. Thus, following the convention of Kolawole et al. (2021), since Rift 1 is located in the flank of Rift 2 in our model setup, Rift 1 serves as the propagator and Rift 2 the receiver segment across their intervening RIZ, whereas, at the underlapping oblique RIZ, both rifts 1 and 2 serve as propagator and receiver segments. Note that during the model run, the underlapping oblique convergent RIZ evolved into a tip-to-tip oblique RIZ geometry.

2.3. Modeling Static Tectonic Stress Distribution

Although the Fastscape algorithm can project a topography at the end of a model run, it is limited in that it cannot resolve the static stress field associated with tectonic deformation. This is relevant for understanding the influence of compounding stress distribution on the displacement field observed in the landscape evolution model. Thus, we simulate the static Coulomb stress distribution across the modeled RIZ geometries, using the same input parameters of model domain size, fault geometry, and kinematics as in the landscape evolution model, and we implement the simulation in Coulomb 3.3 available from USGS website (Toda et al., 2005; Lin, and Stein, 2004). The software utilizes an elastic half-space model to calculate static stress changes in space and time within a model domain due to slip on a given source fault. The general Coulomb stress change formulation is as follows:

$$\Delta\sigma_c = \Delta\tau_s + \mu'\Delta\sigma_n \quad (3)$$

Where $\Delta\sigma_c$ is the Coulomb stress change, $\Delta\tau_s$ is the shear stress change, and $\Delta\sigma_n$ is the normal (clamping) stress change on receiver normal faults due to slip on a source normal fault, and μ' is the

effective coefficient of friction on the faults. We use μ' of 0.55, appropriate for the southern Malawi region (Williams et al., 2019), and fault rupture depth of 5 km. We use the total fault slip in 5 Myr as prescribed displacement on fault plane and model cases involving the activation of each border fault as the source fault while other faults act as the receiver faults; then, we model a single case in which all the border faults are the source faults (i.e., all rupture in the same event) and calculate stress change on N-S strike faults with a rake of -90. For simplicity, each fault is represented as a single rectilinear planar surface. By implementing the static stress model, we can assess the predominant type of Coulomb stress change (i.e., positive or negative) that is transferred into an oblique overlapping divergent rift interaction zone area versus tip-to-tip rift interaction zone.

2.4. Model Limitations

The active northeastern border fault system of the Lower Shire Graben (Thyolo-Muona-Ruo Fault System) is characterized by a staggered, side-stepping geometry that developed over multiple rift phases (Kolawole et al., 2022; Figures 3a-b). Similarly, a major strand of the western border fault system of the Zomba Graben (Lisungwe Fault) shows zig-zag geometry (Figures 3a-b). However, for simplicity, we implemented this fault system as a single planar through-going fault in our model (Figure 5c). We assume the modeled faults have a uniform tip propagation and extension rates due to lack of constants on the timing and rate of fault slip rates. We note a limitation of the poor constraints of fault slip rates in southern Malawi and the shorter duration of model tectonic extension versus nature. We note that although our model uses a constant rainfall rate throughout the model run, paleoclimate studies in the region (e.g., Scholz et al., 2007; Beuning et al., 2011; Konecky et al., 2011; Dulanya et al., 2014) show records of alternating wet and dry periods in as low as 100-year intervals. The limited constraints on fault slip rates, rainfall rates, and the paleotopographic (pre-rift) variations might have resulted in the mismatch between the absolute values of surface elevation in southern Malawi and those in our model results.

We do not implement the NNW-rotation of the northwestern tip of the Thyolo Fault as it is found to have been controlled by the Precambrian basement metamorphic fabrics (Kolawole et al., 2021a). We also acknowledge that the static Coulomb stress change model only assumes a single instance of slip involving the rupture of an entire border fault and does not capture the very complex interactions of border and intrabasinal fault segments over the many cycles of earthquake activity in active rift basins (e.g., Njinju et al., 2022).

3. Results

3.1. Fault Kinematics along the Zomba – Lower Shire - Nsanje Graben System

Field observations of fault-slip striae on exposed fault surfaces in the Zomba, Lower Shire, and Nsanje grabens (Table 1; Figures 6a-g) show a strong component of normal slip on the faults, but with the Nsanje data showing a relatively high obliquity. This is given by the 301°/52° striae (average trend/plunge) on the Zomba Fault slip surface (189°/54° strike/dip; Wedmore et al., 2020b; Figures 8a-b), 231°/80° striae (trend/plunge) on the Thyolo Fault slip surface (160°/69°SW strike/dip; Figures 6c-d), and 193°/44° striae (trend/plunge) on the Nsanje Fault slip surface (059°/79°SE

strike/dip; Figures 6e-g). However, these slip vectors, altogether produce a kinematic strain tensor of 023.3°/69.1° P-axis and 260.3°/11.8° T-axis, suggesting a predominantly normal faulting regime, although with a very minor strike-slip component. The 260.3° (80.3°) (ENE-WSW) T-axis trend is parallel to the known regional geodetically resolved tectonic extension azimuth of 086° ± 5° (Stamps et al., 2008, 2018; Figure 3a) and the regional σ_3 stress direction of 072° ± 14° from earthquake focal mechanism inversion (Williams et al., 2019). Similarly, the strain tensor solution is consistent with the largely normal faulting style of focal mechanism solutions of the recent earthquakes in the Nsanje RIZ (i.e., northern tip of the Nsanje Graben and southeastern tip of the Lower Shire Graben) and those in the Middle Shire RIZ (i.e., southern tip of the Zomba Graben) (Figures 3a-b). These results constrain the normal slip kinematics imposed on the faults in our landscape evolution model.

Table 1. Field data on slip vectors on border faults used for the kinematic tensor calculation.

Rift Basin	Border Fault	Strike/Dip	Plunge/Trend	Source
Zomba Graben	Chingale Step F.	189°/54°	52°/301°	Wedmore et al. (2020b)
Lower Shire Graben	Thyolo F.	160°/69°	80°/231°	This study
Nsanje Graben	Nsanje F.	059°/79°	44°/193°	This study

3.2. Overlapping Oblique RIZ: Model Displacement Field, Rift Topography, and Drainage Morphology

After 5 Myr of model run, Rift 1 had propagated into the footwall of Rift 2 and the western border fault of Rift 1 is hard-linked with the northeastern border fault of Rift 2 across their intervening overlapping oblique RIZ (Figure 7a). The integrated fault displacement rate fields represent distribution of rift basin subsidence and flank uplift in RIZs. Particularly, Rift 1 is characterized by uniform displacement ellipses on its two border faults with up to 0.12 mm/yr footwall uplift rate, ca. 0.2 mm/yr maximum hanging wall subsidence rate. At the overlapping RIZ, the southern tip of Rift 1 extends into a narrow region that is dominated by background displacement rate of ca. 0.03 mm/yr or less. To the south of the RIZ, the northeastern border fault of Rift 2 shows a more pronounced hanging wall subsidence rate of >0.32 mm/yr. At the region of hard-linkage with the western border fault of Rift 1, the fault shows a localized zone of significant displacement rate at the western margin of the RIZ, defined by the region of fault intersection. More specifically, the localized subsidence occurs at the intersection of the southern extension of Rift 1's western border fault with the northwestern extension of Rift 2's northeastern border fault. Also, we note that, in general, Rift 2 shows a greater axial subsidence rate (0.12 - 0.16 mm/yr) than Rift 1 (0.04 - 0.08 mm/yr).

The topography of RIZs is largely modified by the rift fault propagation, resulting in distinct topography and drainage pattern due to different types of RIZs. The surface topography of the overlapping oblique RIZ shows a narrow, uplifted block of up to 12 - 25 m, and the rift lake in Rift 2 is deepest (ca. 40 m) to the south of the uplift (Figure 7b), consistent with the patterns in the displacement field map (Figure 7a). Although the drainage system is characterized by well-developed

rift lakes in rifts 1 and 2, the lakes remain disconnected across the overlapping RIZ (Figure 7c). These results indicate that rifts 1 and 2 remain as isolated basins and their fluvio-lacustrine depositional environments disconnected from each other. The cross-sectional view of rift structure across the RIZ features a paired graben-half graben morphology in which there is a significantly exposed basement at the rift floor with a graben structure to the west and half graben to the east (cross-section B-B' in Figure 7d). Also, the section shows a thinner syn-rift cover (ca. 5 m) on the hanging wall of Rift 1's eastern border fault and a thicker cover (up to ca. 40 m) on Rift 2's eastern border fault. In the region of transition from the overlapping RIZ into Rift 2, the model shows the presence of a prominent isolated depression at the top-basement surface which is also represented at the model top-syn-rift sediment surface (Figure 9a); this represents the fault intersection-related depocenter that developed early and continued to be active with progressive tectonic extension.

However, at the end of 10 Myr model run, the displacement field results show that the southward propagating tip of Rift 1 has finally breached the overlapping RIZ, and the rifts are now structurally hard-linked and coalesced across the RIZ (Figure 8a). In addition, both the surface topography and drainage system (Figures 8b-c) show that the depositional environments of rift basins 1 and 2 are now fully connected, and that a through-going axial rift floor has been established across the RIZ. Moreover, the model results also show that the displacement rates on the border faults have now decreased due to the overlapped uplift and subsidence, and that the zone of rift intersection is now the focus of accelerated displacement (Figure 8a) and surface subsidence (Figure 8b). This zone of focused displacement is the fault intersection depocenter bounded by faults that trend parallel to the border faults of the interacting rift pair.

3.3. Tip-to-Tip Oblique RIZ: Model Displacement Field, Rift Topography, and Drainage Morphology

In contrast to the overlapping RIZ, at the end of the 5 Myr model run, the rift tips of both Rift 2 and Rift 3 have propagated towards each other and their axial depocenters have merged, forming a tip-to-tip oblique RIZ (Figure 7a). The displacement field at the end of 5 Myr presents a different pattern to the one of overlapping RIZ, where the border faults of Rift 3 commonly show a footwall uplift rate of ca. 0.04 - 0.08 mm/yr with a maximum of 0.12 mm/yr, and a hanging wall subsidence rate of up to 0.28 mm/yr. The basin shows an axial subsidence rate of 0.12 - 0.16 mm/yr, similar to Rift 2. More importantly, a depocenter of 0.08 - 0.12 mm/yr subsidence rate extends from the axes of both rifts and merges across the intervening tip-to-tip oblique RIZ. The model result shows the development of localized subsidence at the zone of intersection of the southeastern extension of Rift 2's western border fault with the northern extension of Rift 3's western border fault. Similarly, the southeastern extension of Rift 2's northeastern border fault intersects with the northern extension of Rift 3's eastern border fault (Figures 7a-b). These fault intersections represent a hard-linkage of the border faults, forming a broad obtuse angled hanging wall sub-basin along the eastern margin of the RIZ and a reflex angled sub-basin along the western margin. The reflex-angled linkage zone localized more subsidence rate (up to 0.24 mm/yr) which decreases eastward to 0.08 in the obtuse-angled linkage zone.

In the tip-to-tip RIZ, the basinal surface topography features a wide low elevation area (ca. 12 m) which deepens westward to ca. 30 m in the reflex-angled linkage zone (Figure 7b). The model drainage map (Figure 7c) shows that the rift lakes of Rift 2 and Rift 3 are connected across the RIZ and deepen from 12 m, westward to ca. 25 m in the western reflex-angled RIZ margin. In essence, the fluvio-lacustrine depositional environments of the two rifts have linked and become open to one another. The cross-section of the model tip-to-tip RIZ shows a west-dipping asymmetric graben morphology, an absence of basement exposure, and a syn-rift sedimentary wedge that thickens from ca. 10 m at the eastern margin to ca. 30 m at the western margin of the RIZ (cross-section C-C' in Figure 7d).

Along the axes of the model rift zones, the variation in top-synrift sedimentary surface relief mimics that of the top-basement relief (Figure 9a). The syn-rift fill of model Rift 1 thins southwards and the surface onlaps the basement exposures of the overlapping oblique RIZ. South of the RIZ, the model surface drops steeply into Rift 2, at a location wher the syn-rift cover sequence is thickest among all three rifts. Interestingly, although the basement is buried across the tip-to-tip oblique RIZ, there exists a broad upwarp at the top-basement above which the syn-rift sequence also defines a structural-high. Also, the model tip-to-tip RIZ shows an isolated depression at the top-basement surface, but which is non-existent at the model top-syn-rift sediment surface (Figure 9a); this represents the fault intersection-related depocenter that developed early, and later became buried as the rift tips coalesced across the RIZ.

Overall, prior to the coalescence of the rifts (10 Myr time step, Figure 8), the comparison of the along axis relief morphology styles across the rift interaction zones in the initial model time step and the study area (Figures 9a-b) shows a correlation of 'steep' topographic down-step across the overlapping oblique RIZ and a gentle surface arching across the tip-to-tip RIZ. However, we note that the absolute values of model surface displacement or elevation are not the same as those of the natural RIZ (Figures 9a-b), likely due to the poor constraints on the slip rate on border faults from the southern Malawi, paleotopography, and possibly the imposed constant rainfall rates and duration of tectonic extension in the models. The model predicts that there is no exposed basement across the tip-to-tip RIZ, whereas natural observation shows the presence of a minor exposure of the basement within the RIZ (Figure 9a). In addition, the model predicts that the rift depocenters are yet to link across the overlapping RIZ, which contrasts with the Middle Shire RIZ across which the Shire River connects the Zomba and Lower Shire grabens (Figures 3a-b).

The 10 Myr timestep shows a paleo-rift interaction zone across which rift coalescence is even more advanced than it was at the 5 Myr timestep (Figures 8a-c). However, similar to the overlapping RIZ, the tip-to-tip RIZ also shows a focusing of greater displacement rates and subsidence at the intersection zone of the border faults and relatively lower displacement rates on the border faults themselves (Figures 8a-b).

3.4. Predicted Static Tectonic Stress Distribution across the RIZs

The modeled stress field shows different patterns between tip-to-tip oblique RIZ and overlapping oblique RIZ. In each case of single border fault rupture (Figures 10a-f), the regions of positive Coulomb stress change (stress concentration) are at the tips of the faults, and the regions of negative Coulomb stress change (stress relaxation) are in the hanging wall and footwall of the faults. Across

the overlapping RIZ, the lobes of stress concentration at the southern tips of Rift 1 border faults (faults 1 and 2) generally extend into the footwall of Rift 2's northeastern border fault (Figures 10a-b). The proximity of the southern tip of Rift 1's western fault (fault 2) to the northern tip of Rift 2's northeastern fault (fault 3) allows for the repeat stress concentration events at the intersection zone of the two border faults (Figures 10b-c).In contrast, the lobes of stress concentration at the southern tip of Rift's eastern fault (fault 1) always only intersect with the large lobe of stress relaxation in the footwall of Rift 2's northeastern fault (fault 3) (Figures 10a and 10c). Coulomb stress change transfer to fault 3 due to slip on fault 1 shows a minor increase, mainly focused onto the central section of fault 3's slip surface (3-D fault plane view in Figure 10a). In contrast, stress change transfer to fault 3 due to slip on fault 2 shows significant increase, and it is focused onto a large portion of northwestern slip surface of fault 3 (3-d fault plane view in Figure 10b).

Across the tip-to-tip RIZ, all events of slip on any of Rift 2 and Rift 3's border faults (faults 3 to 6) concentrate positive Coulomb stress changes in the RIZ (Figures 10c – 10f). The lobes of positive stress change transfer due to slip on Rift 2's border faults (faults 3 and 4) extend onto the northern tips of Rift 3's border faults (faults 5 and 6). Similarly, the lobes of positive stress change transfer due to slip on faults 5 and 6 extend far onto the southwestern sections of Rift 2's faults 3 and 4. Overall, the results can be summarized in a single model case where all the faults are activated as source faults (Figure 10g), showing that the overlapping RIZ is largely a zone of stress relaxation and the tip-to-tip RIZ a zone of compounded stress concentration.

4. Discussion

4.1. Comparison of Model Results with Natural Observations

4.1.1 Rift Interaction Zone Morphology

The general patterns of the surface and top-basement displacement and drainage morphology of the model RIZs (Figures 9a-b) provide important insights relevant for understanding the structure and pace of evolution of the Middle Shire RIZ and Nsanje RIZ. In the model, at sometime during the propagation of the rifts (e.g., the 5 Myr time step), unlike the tip-to-tip RIZ, the rift floor of overlapping RIZ retained widespread basement exposure, which is consistent with the current widespread exposure of the Precambrian basement in the Middle Shire RIZ. Similarly, the broad upwarp of the model syn-rift surface across the model tip-to-tip RIZ is collocated with the region of upwarp in the long wavelength surface elevation across the Nsanje RIZ (Figures 9a-b). The model shows an early coalescence of the rift axial lakes across the tip-to-tip RIZ, consistent with the extension of a wetland drained by the Shire River across the Nsanje RIZ (Elephant and Ndindi Marshes, Figures 3a-b, 4d, 7c). Overall, in contrast to the tip-to-tip RIZ, the model predicts delayed coalescence of the depositional environments across the overlapping oblique divergent RIZ (see disconnected rift lakes in Figure 7c). In nature, although the depositional environments of the Zomba and Lower Shire grabens are already connected (Shire River flows across the Middle Shire RIZ; Figure 3a), published geomorphological analysis and knickpoint age estimates suggest a recent (Mid. Pleistocene) breaching of the Middle Shire RIZ (Kolawole et al., 2021a; Dulanya et al., 2022) relative to the Late Oligocene initiation of Cenozoic rifting in the region (Ojo et al., 2022a). Furthermore, both the model and natural

surface relief show the presence of the broad topographic 'step' from the Zomba Graben (Rift 1) into the Lower Shire Graben (Rift 2) (Figures 9a-b).

The Bouguer gravity model of the Lower Shire Graben (WGM2012; Bonvalot et al., 2012; Figures 9b, S3) shows a prominent rift-parallel gravity-low (ca. 25 mGal) anomaly near the center of the basin. This anomaly has been observed in published airborne gravity map of the graben, interpreted to represent a deep depocenter in the basin (Ngabu depocenter; Chisenga et al., 2018). This gravity-low anomaly is colocated with a zone of localized >2.5 km subsidence on the hanging wall of the buried southern Mwanza Fault along the axis of the Lower Shire Graben which records multiple phases of tectonic extension (Kolawole et al., 2022). To the southeast, this gravity-low anomaly transitions into a broad rift-orthogonal gravity-high (ca. 92 mGal) anomaly extending far into the Nsanje RIZ, which then decreases again to <85 mGal in the Nsanje Graben (Figure 9b; Figure S3). Similarly, the along-rift variation in the trend of the basement depth (Figure 9b) shows decreasing basement depths towards the southeast. Both the aeromagnetic basement depth and gravity anomaly trends, together suggest that the basement shallows into the Nsanje RIZ and deepens southwards into the Nsanje Graben (Figure 9b). The results indicate that there exists a shallowly-buried basement-high beneath the Nsanje RIZ, which is also predicted by the model in the tip-to-tip RIZ (Figure 9a).

Our interpretation of shallow basement burial in the Nsanje RIZ is reflected by the relatively small vertical surface offset on the Ruo Fault (i.e., escarpment height; Figure S2), the broad upwarp of the surface topographic relief across the RIZ (low-pass filtered SRTM plot in Figure 9b), and the restricted basement exposure on the rift floor (Figures 3b, 4c-d, 9b). Interestingly, the Nsanje RIZ surface tilts and deepens to the west without any visible surface fault scarp at the western margin of the RIZ (Figures 4c-d, S2). We speculate that the westward tilting and deepening of the Nsanje RIZ is likely due to the presence of a blind active NW-trending NE-dipping fault near the western margin of the RIZ (see dashed fault in Figures 4c, S2). Potentially, higher slip rates on this blind fault relative to the Ruo Fault could have created the apparent half-graben geometry of the RIZ, in which the Ruo Fault hanging wall is on the 'uplifted' margin. The uplift of the northeastern margin of the RIZ relative to the southwestern margin is highlighted by the presence of incising west-flowing transverse streams that cut into the hanging wall of the Ruo Fault (map in Figure S2).

The inferred blind fault at the SW margin of the Nsanje RIZ may be responsible for some of the earthquake clusters in the Nsanje RIZ (see Figure 3a) but likely remains blind due to sedimentation rates outpacing the slip rate on the fault. Modern fault slip rates are generally considered to be low in southern Malawi, but quantitative constraints are lacking (Williams et al., 2022). Also, there is no quantitative constraint on sedimentation rates in the Lower Shire Graben due to the absence of high-resolution subsurface imaging and well controls. However, the Shire River is a major river that drains the region and channels large amounts of sediments into the Lower Shire and Nsanje grabens and represents a major sediment contributor to the Zambezi River with the Mozambique Channel being the being the sink of the river system (e.g., Dulanya et al., 2022; Garzanti et al., 2022). Furthermore, the high sedimentation inference is supported by the broad swampy terrain of the southwestern margin of the Nsanje RIZ (Figure 4d) being dominated by the Shire River flood plains and the Elephant Marsh beneath which the fault is located (Figures 4c-d). In summary, at some time in the past, the currently buried basement-high beneath the Nsanje RIZ sediments should have been a broad exposed basement arch that may have isolated the Lower Shire Graben from the Nsanje Graben. With

progressive tectonic extension and rift propagation into the RIZ, this elevated basement block subsequently experienced down-faulting, erosion, and burial; a process which facilitated the structural breaching of the RIZ and linkage of the two rift basins (Kolawole et al., 2021a).

4.1.2 Significance of Fault Intersection for the Deformation of Rift Interaction Zones

The landscape evolution model results predict a localized zone of elevated displacement rates and associated basement subsidence at the western margin of the overlapping divergent RIZ, and another one at the western margin of the tip-to-tip oblique RIZ, both colocated with regions of fault intersection (Figures 7a-b, 7d, and 9a). We interpret this modeled subsidence to be consistent with the development of isolated fault-bounded depocenters in the Middle Shire RIZ and the potential presence of a blind high-strain fault in the western margin of the Nsanje Graben. Near the western margin of the Middle Shire RIZ, the surface geology shows the presence of a ca. 17 km^2 isolated depocenter of Quaternary sediments, herein referred to as the 'Neno depocenter' (Figures 3b). This localized depocenter is elongate, NW-trending, and fault-bounded. It sits at the intersection of the southern extension of the NNE-trending Lisungwe Fault and a NW-trending fault that trends parallel to the Thyolo border fault of the Lower Shire Graben (Figure 3b). The basement subsidence is caused by overlapped and enhanced displacement of rift faults, implying the possible control on the formation of its natural equivalent, the Neno depocenter. Moreover, the topographic surface of the depocenter is relatively 'smoother' than the surrounding basement-dominated topography (Figure 3a), consistent with a dominance of unconsolidated sediments.

Just south of the Neno depocenter, in Majete, we observe an even broader (ca. 42 km^2) NW-trending fault-bounded area with similar surface smoothness as the Neno depocenter, possibly representing an incipient localized depocenter (Figures 3b-c). This potential depocenter in Majete sits at the intersection of the southern extension of the NNE-trending Wamkurumadzi Fault and a NW-trending fault parallel to the Thyolo Fault. The cross-sectional topographic relief profile of the RIZ (Figure 4a) shows a ca. 35 km-wide graben structure, with a surface that deepens towards the Lisungwe and Wamkurumadzi faults to the west and is bounded to the east by a system of NW-trending faults. Generally, both antithetic and synthetic fault linkage create localized amalgamated depocenters on the hanging wall of both faults (synthetic interaction, Figures 7a, 8a) or in the hanging wall of the dominant fault segment (antithetic interactions; Figures 7a, 7d inset; Duffy et al., 2015). The depocenters are often well represented as prominent anomalies in the throw-distance (T-x) profiles of the interacting faults with their characteristic abrupt 'throw steps' (3-D sketch and T-x plots in Figure 7d inset; Duffy et al., 2015). However, based on insights of fault intersection depocenters from our modeling results (Figures 7-8), we interpret these isolated fault-bounded depocenters in the Middle Shire RIZ to be distributed local subsidence zones that are controlled by the intersection and interaction of fault segments extending from the Zomba and Lower Shire rifts into the RIZ. Notably, recent analog models of linkage between obliquely-oriented rifts show linkage of antithetic faults at the propagating fault tips (Schmid et al., 2023).

On the dominant dip of faults that host the fault intersection depocenters, we note that the overlapping divergent RIZ model results present the fault intersection-related depocenter to be localized on a NW-dipping fault; whereas natural observations show the isolated depocenters in the

Middle Shire RIZ to be localized on NE-dipping faults. We suggest that the inherited heterogeneity of the pre-rift basement of the Middle Shire RIZ may play an important role in determining the dominant fault dip direction, which our models are not designed to assess. Nevertheless, the model results suggest that localities of fault intersection within deforming RIZs are zones that localize subsidence where significant tectonic strain associated with progressive rift linkage may accumulate. Further, these fault intersection zones are zones where strain is transferred between the interacting rift tips as they propagate across a deforming RIZ. The early localization of subsidence in the model tip-to-tip RIZ is facilitated by the early intersection of propagating border fault tips into the RIZ, and the model predicts that even during the advanced stages of rift coalescence, the continued deepening of the RIZ sub-basin is most intense in the location of the early fault intersection depocenter (Figure 7d). Thus, we suspect that westward deepening of the Nsanje RIZ could be indicative of either the presence of a buried fault intersection-related localized depocenter or a NW-trending, NE-dipping normal fault at the southwestern margin of the RIZ. This may possibly be facilitating the incursion of wetlands (Elephant Marsh) from the Lower Shire Graben into the western margin of the Nsanje RIZ (Figures 3a-b, 4c-d). Altogether, the landscape evolution model results and natural observations suggest that after the structural breaching of a rift interaction zone (i.e. post-rift linkage), rift coalescence is initiated by the localization of distributed incipient depocenters as overlapped hanging wall subsidence. Such depocenters may preferentially develop at localities of fault-intersection within the RIZ.

4.1.3 Tectonic Stress Transfer and Active Faulting in the Rift Interaction Zones

The seismicity patterns in the region reflect relatively greater clustering of earthquakes in the Nsanje RIZ compared to the Middle Shire RIZ (Figures 3a-b). The clustered events in the Nsanje RIZ includes a Mw 5.5 event and its aftershocks that likely ruptured the Ruo Fault and the northern extension of the Nsanje and Ndindi faults. The largest magnitude events in the Nsanje RIZ (Mw 5.5 and Mw 4.9; source: USGS earthquake catalog) occurred near the eastern margin of the RIZ. The focal mechanism nodal planes generally trend N-to-NNW and NW, the former being parallel to the trend of the Nsanje Graben border faults (Nsanje and Ndindi faults), and the latter being parallel to the trend of the Ruo border fault segment (Figures 3a-b). These seismicity patterns likely reflect a more pronounced active crustal deformation with significant moment release, and a localization of brittle strain within the Nsanje RIZ. Although instrument records show the occurrence of at least one Mw>5 event in the Middle Shire RIZ (Figure 3a), the events seem relatively more sporadic than those in the Nsanje RIZ.

The Coulomb static stress transfer models predict a concentration of positive Coulomb stress changes within the tip-to-tip RIZ produced by normal slip on the rift border faults, which contrast the case of overlapping oblique divergent RIZ where a colocation of positive and negative stress changes is predicted (Figure 8). In essence, in the tip-to-tip RIZ, the propagating rift tips grow into a zone of stress concentration within the RIZ, whereas, in the overlapping divergent RIZ, the propagating rift tip grows into a zone of stress relaxation. These results highlight the significant role of border fault dip polarity in determining how static stress changes are transferred across deforming RIZs. Indeed, antithetic dips of interacting border faults inhibit stress concentrations, compared to synthetically interacting border faults. The long-term compounding effect of stress relaxation in overlapping RIZs

suggests that such RIZs host a persistent stress shadow where strain relaxation dominates. Altogether, these model results suggest that over the repeated cycles of fault slip events at the propagating rift tips, the time-averaged brittle strain accumulation will likely be greater in tip-to-tip RIZs than in overlapping divergent RIZs. Although the constraints on fault slip history is sparce, we can still interpret that depending on RIZ geometry, a RIZ may localize compounding stress concentration, favoring rapid rift linkage and coalescence as in the case of tip-to-tip RIZs, or may experience compounding stress relaxation, favoring delayed rift coalescence, as in the case of overlapping divergent RIZs.

The southern tip of the Zomba Fault appears to be 'stagnated' as it does not extend across the entire Middle Shire RIZ (Figure 3a) relative to the western border fault system of the Zomba Graben (Lisungwe-Wamkurumadzi fault system) which has propagated close to and is soft-linked with the northeastern border fault of the Lower Shire Graben (Thyolo Fault, and its subsidiary footwall faults) (Figure 3a). We suggest that the attainment of hard linkage between the Lisungwe-Wamkurumadzi and Thyolo faults can be explained by positive Coulomb stress change transfer onto the Thyolo Fault surface due to slip on the Lisungwe-Wamkurumadzi fault system. The Coulomb stress change transfer calculations show that slip on the Zomba Fault is not able to transfer significant positive stress change onto the Thyolo Fault plane across the overlapping RIZ (3-d plot in Figure 10a). In contrast, the proximity of the tips of fault 2 (representing Lisungwe-Wamkurumadzi fault system) and fault 3 (representing Thyolo Fault) predicts compounding stress concentration in the area between the northwestern end of the Thyolo Fault and southern ends of the Lisungwe and Wamkurumadzi faults (Figures 10a-b). Thus, the interaction of the fault tips allows the localization of brittle deformation, facilitating the northwestward propagation of the Thyolo Fault and breaching of the RIZ. The two fault systems are hard-linked by a cluster of NW-to-NNW-trending fault clusters, guided by the NW-SE to NNW-SSE rotation of the pre-rift basement metamorphic fabrics (Kolawole et al., 2021a).

4.2. Controls of Rift Interaction Zone Geometry on Early vs Delayed Rift Coalescence

The striking contrast in the stages of evolution of the two model RIZs at the end of the 5 Myr (relative to the 10 Myr) model runs, and the observations of present-day natural rift morphology at the Middle Shire and Nsanje RIZs (e.g., Figures 9a-b) provide compelling evidence for a difference in the pace of rift linkage with variation in RIZ geometry. This interpretation agrees with the predicted patterns of crustal stress distribution across overlapping divergent (antithetic border fault interactions) and tip-to-tip RIZs (synthetic border fault interactions) (Figure 10). The results predict delayed rift coalescence across an overlapping divergent RIZ and demonstrate that it can be explained by the propagation of rift tips into a persistent stress relaxation zone in the RIZ. Although the persistent footwall uplift of the flank of the 'receiver' rift segment (e.g., Rift 2) inhibits subsidence across the overlapping divergent RIZ, the kinematic opening direction of such a rift induces compression that acts normal to the direction of growth of the 'propagator' rift segment tip (i.e., southern tip of Rift 1). Thus, compression normal to rift tip propagation direction can also contribute to a delayed advancement of the 'propagator' rift tip into the overlapping divergent RIZ. This is consistent with observations of stagnation of propagating mid-oceanic ridges by compressive tectonic loading in the direction of ridge propagation (Le Pourhiet et al., 2018).

Strong crustal blocks beneath a RIZ, either crustal-scale or only in the lower-crust, can inhibit rapid propagation of a rift tip (Van Wijk and Blackman, 2005; Le Pourhiet et al., 2018). However, this is not likely to be the case in our study area as basement geologic maps (e.g., Bingen et al., 2009; Fritz et al., 2013; Thomas et al., 2022) and large-scale basement metamorphic fabric trends (Kolawole et al., 2021a, 2022) of the region do not show the presence of a discrete basement block separating the southern Malawi Rift from the Lower Shire Graben. However, numerical models show that significant activation of rift stalling by lower crustal rheological blocks is in fact, most significantly activated when there is compressive tectonic loading ahead of the propagating rift tip (Le Pourhiet et al., 2018). Also, regional weak lower crust beneath interacting rifts and their intervening RIZ may also delay rift linkage, and low surface erosional efficiency may delay the coalescence of depositional environments of interacting rifts (Wolf et al., 2022). Nonetheless, although the Nsanje RIZ developed over the NE-trending Precambrian Lurio Shear Zone (Kolawole et al., 2022), there is no evidence on the lower crustal property of the shear zone that might suggest that it is significantly stronger than the lower crust of the Middle Shire RIZ. Therefore, we cannot strongly claim that some unknown lower crustal character influenced the delayed rift linkage and coalescence across the Middle Shire RIZ.

Thus, we argue that in non-volcanic active rift settings, the geometry of rift interaction zones strongly influences the pace of rift linkage and coalescence by modulating the overall static stress distribution and tectonic loading patterns across the RIZ. As a consequence, RIZ geometry may modulate the evolution of the syn-rift depositional environment, as well as patterns of landscape evolution in actively deforming zones of rift interaction. This was initially speculated in Kolawole et al. (2021) based on conceptual understanding of a transition from a surface topographic basement-high RIZ into a 'flat' sediment-covered area defining a paleo-RIZ. It was also speculated that paleo-RIZs can be identified by the presence of buried large basement blocks at zones of lateral changes in the along-trend geometry of a continental rift or rifted margin (Kolawole et al., 2021a). However, this current study provides natural and model examples that validate these speculations, as well as a detailed evaluation of how RIZ geometry may control the pace of transformation of a RIZ with progressive tectonic deformation.

Models of rift propagation commonly test for the controls of extension direction (i.e., oblique versus orthogonal) on the deformation patterns across rift interaction zones (e.g., Brune, 2014; Zwaan and Schreurs, 2017; Zwaan et al., 2022). However, little is known of the control of the relationship between obliquity of extension on the pace of lateral rift propagation and linkage of interacting rift segments. Although our study is primarily focused on a rift zone with predominantly normal faulting kinematics (Figure 6h; Williams et al., 2019), we note that it is also possible that the appreciable strike-slip component of slip on the Nsanje Fault (Figure 6g) may have promoted the rapid lateral propagation of the rift into the Nsanje RIZ. Overall, we think that the observations and model results in Middle Shire and Nsanje RIZs can be applied to RIZs elsewhere. For example, the ca. 750 km-long Malawi Rift and 730 km-long Tanganyika Rift exhibit greater rift lengths than many other rift segments in the East African Rift System. The two rifts were proposed to have evolved over multiple pulses of lateral propagation (e.g., Specht and Rosendahl 1989; Scholz et al., 2020; Kolawole et al., 2021a; Shaban et al., 2023). The Kavala Island Ridge, buried beneath the central Tanganyika Rift, is an example of a basement block at which rift segments define overlapping RIZ geometry, and in which their border faults define a divergent overlapping transfer zone (Specht and Rosendahl 1989; Morley et al., 1990; Muirhead et al., 2018; Shaban et al., 2023). This ridge is argued to be a long-lived structural-high in

778 the Tanganyika Basin, which served as a paleo-drainage divide during periods of lowstands (Scholz
779 and Rosendahl, 1988; Shaban et al., 2023). Such large structurally controlled paleo-drainage divides
780 commonly modulate biodiversity patterns in active continental rift environments (e.g., Russell et al.,
781 2012; Dommain et al., 2022), demonstrating the roles of RIZ evolution on sedimentary depositional
782 environment, landscape evolution, and floral and faunal speciation gradients.

783 Similarly, along the Malawi Rift, published maps of the basement topography (Specht and Rosendahl,
784 1989; Scholz et al., 2020) reveals the presence of a large 4,700 km^2 basement-block, the 'Likoma-
785 Lipichilli Block', buried beneath younger syn-rift sediments in the central section of the rift. This
786 basement block separates the northern Malawi Rift from the southern Malawi Rift and could have
787 represented a major structural-high on the paleo-topography of the rift, possibly serving as a paleo-
788 drainage divide during periods of low stands. For example, the block is collocated with an inferred
789 earlier termination zone of the northern Malawi Rift during the long-term southward growth of the
790 rift (Scholz et al., 2020).

791

792 **Conclusions**

793 We applied geologically constrained landscape evolution and static stress models to evaluate the
794 surface processes and stress state in two contiguous non-volcanic rift interaction zones of contrasting
795 end-member rift interaction zone (RIZ) geometries, the Zomba - Lower Shire - Nsanje graben system
796 at the southern branch of the East African Rift System. The Middle Shire RIZ is an overlapping
797 oblique divergent RIZ in which the NNE/N-trending southern Malawi Rift is propagating into the
798 NE shoulder of the NW-trending Lower Shire Graben, where widespread basement exposure
799 dominates the rift floor. The Nsanje RIZ is a tip-to-tip oblique RIZ in which the Lower Shire Graben
800 has propagated into the northern tip of the N-trending Nsanje Graben, where the rift floor is
801 dominated by widespread sediment deposition with minor basement exposure.

802 In general, the landscape evolution model results provide insights into the evolution of surface
803 morphology and rift structure across the RIZs in the study area. The model results show that with
804 progressive extension and tip growth, the overlapping oblique divergent RIZ maintains minor
805 basement down-throw and an unequilibrated axial stream profile, which contrasts the widespread
806 basement burial and equilibrated axial stream profile across tip-to-tip RIZ. Further, static tectonic
807 stress distribution models suggest compounding stress concentrations at tip-to-tip RIZs, thus implying
808 that brittle strain localization and rift coalescence is favored in such RIZs. In contrast, the model
809 predicts compounding stress relaxation at overlapping oblique divergent RIZs, favoring stalled rift
810 coalescence, and providing kinematic explanation on the distribution of deformation in these two
811 RIZs. These findings indicate that antithetically interacting border faults inhibit stress concentration
812 within RIZs, and that synthetically interacting border faults are stress concentrators within their
813 intervening RIZs. The results show that the kinematics of the rift border faults across the overlapping
814 divergent RIZ induces compression normal to the rift tip propagation direction, promoting delayed
815 advancement of the 'propagator' rift tip into the overlapping RIZ. Thus, we argue that in the absence
816 of magmatism, RIZ geometry strongly influences the pace of rift coalescence by modulating the spatial
817 distribution of tectonic stresses necessary to promote rift-linking deformation. The field observations
818 and model results in Middle Shire and Nsanje RIZs presented in this study provide a better

understanding of how the geometry rift interaction zones elsewhere may influence the pace of rift linkage and coalescence.

Acknowledgements

We thank Elizabeth Catlos for the editorial handling of our paper, and reviewers Bailey Lathrop and two anonymous reviewers for their comments and suggestions that have helped to improve the quality of the manuscript. Thanks to Chikondi Chisenga for assisting during the field work. We also thank the Columbia Climate School for providing the research funds that supported the field component of this project.

Author contributions

F.K. and L.X. conceptualized the project. F.K. performed the fieldwork. L.X. conducted the numerical modelling. F.K. and L.X. interpreted the results. F.K. wrote the manuscript. L.X. and Z.D. revised the manuscript.

Data Availability

All the datasets supporting the analysis performed in this work are either already in public domain or provided in the manuscript, and none are proprietary. Fastscape is available via zenodo (DOI: 10.5281/zenodo.4435110). Coulomb 3.3 is accessible from USGS (https://pubs.usgs.gov/of/2011/1060/).

References

Aanyu, K. and Koehn, D. (2011). Influence of pre-existing fabrics on fault kinematics and rift geometry of interacting segments: analogue models based on the Albertine Rift (Uganda), Western Branch-East African Rift System. Journal of African Earth Sciences, 59(2-3), pp.168-184.

Agar, S.M. and Klitgord, K.D. (1995). Rift flank segmentation, basin initiation and propagation: a neotectonic example from Lake Baikal. Journal of the Geological Society, 152(5), pp.849-860.

Barr, M.W.C., Brown, M.A. (1987). Precambrian gabbro–anorthosite complexes, Tete Province, Mozambique. Geol. J. 22 (S2), 139–159.

Beuning, K. R. M., Zimmerman, K. A., Ivory, S. J., and Cohen, A. S. (2011). Vegetation response to glacial–interglacial climate variability near Lake Malawi in the southern African tropics. Palaeogeography, Palaeoclimatology, Palaeoecology, 303, 81–92.

Bicca, M.M., Jelinek, A.R., Philipp, R.P. and Jamal, D.L. (2019). Mesozoic-Cenozoic landscape evolution of NW Mozambique recorded by apatite thermochronology. Journal of Geodynamics, 125, pp.48-65.

Bingen, B., Jacobs, J., Viola, G., Henderson, I.H.C., Skår, Ø., Boyd, R., Thomas, R.J., Solli, A., Key, R.M., Daudi, E.X.F. (2009). Geochronology of the Precambrian crust in the Mozambique belt in NE Mozambique, and implications for Gondwana assembly. Precambrian Res. 170 (3–4), 231–255.

Bloomfield, K. (1958). The geology of the Port Herald area. Bull. Geol. Surv. Malawi, 9. Zomba.

Bloomfield, K. (1965). The Geology of the Zomba Area, Bull. Geol. Surv. Malawi, 16, 193 pp.

Bonvalot, S., Balmino, G., Briais, A., M. Kuhn, Peyrefitte, A., Vales, Biancale, R., Gabalda, G., Moreaux, G., Reinquin, F. Sarrailh, M. (2012). World Gravity Map, 1:50000000 map, Eds. : BGI-CGMW-CNES-IRD, Paris.

Bosworth, W., 1985. Geometry of propagating continental rifts. Nature, 316(6029), pp.625-627.

Braun, J., & Willett, S. D. (2013). A very efficient O (n), implicit and parallel method to solve the stream power equation governing fluvial incision and landscape evolution. Geomorphology, 180, 170-179.

Bosworth, W., 1985. Geometry of propagating continental rifts. Nature, 316(6029), pp.625-627.

Brune, S., 2014. Evolution of stress and fault patterns in oblique rift systems: 3-D numerical lithospheric-scale experiments from rift to breakup. Geochemistry, Geophysics, Geosystems, 15(8), pp.3392-3415.

Castaing, C. (1991). Post-Pan-African tectonic evolution of South Malawi in relation to the Karroo and recent East African rift systems. Tectonophysics, 191(1-2), pp.55-73.

Chisenga, C., Dulanya, Z., and Yan, J. (2018). The structural re-interpretation of the Lower Shire Basin using edge detection and gravity inversion methods of basement topography. Journal of African Earth Science, 149, 280–290.

Chorowicz, J. (2005). The east African rift system. J. Afr. Earth Sci. 43 (1–3), 379–410.

Cladouhos, T.T. and Allmendinger, R.W., 1993. Finite strain and rotation from fault-slip data. Journal of Structural Geology, 15(6), pp.771-784.

Coffield, D.Q. and Schamel, S., 1989. Surface expression of an accommodation zone within the Gulf of Suez rift, Egypt. Geology, 17(1), pp.76-79.

Corti, G., van Wijk, J., Cloetingh, S. and Morley, C.K. (2007). Tectonic inheritance and continental rift architecture: Numerical and analogue models of the East African Rift system. Tectonics, 26(6).

Croissant, T., & Braun, J. (2014). Constraining the stream power law: a novel approach combining a landscape evolution model and an inversion method. Earth surface dynamics, 2(1), 155-166.

Daly, M.C., Chorowicz, J., Fairhead, J.D. (1989). Rift basin evolution in Africa: the influence of reactivated steep basement shear zones. Geol. Soc. Lond., Spec. Publ. 44 (1), 309–334.

Daly, M.C., Green, P., Watts, A.B., Davies, O., Chibesakunda, F., Walker, R. (2020). Tectonics and Landscape of the Central African Plateau, and their implications for a propagating Southwestern Rift in Africa. Geochem. Geophys. Geosyst. 21.

Daly, M.C., Lawrence, S.R., Kimun'a, D., Binga, M. (1991). Late Palaeozoic deformation in central Africa: a result of distant collision? Nature 350 (6319), 605–607.

Delvaux, D. (1989). The Karoo to recent rifting in the western branch of the East-African Rift System: a bibliographical synthesis. In: Mus. Roy. Afr. Centr., Tervuren (Belg.), D´ept. G´eol. Min., Rapp. Ann, 1990, 1991, pp. 63–83.

Dommain, R., Riedl, S., Olaka, L.A., deMenocal, P., Deino, A.L., Owen, R.B., Muiruri, V., Müller, J., Potts, R. and Strecker, M.R., 2022. Holocene bidirectional river system along the Kenya Rift and its influence on East African faunal exchange and diversity gradients. Proceedings of the National Academy of Sciences, 119(28), p.e2121388119.

Duffy, O.B., Bell, R.E., Jackson, C.A.L., Gawthorpe, R.L. and Whipp, P.S., 2015. Fault growth and interactions in a multiphase rift fault network: Horda Platform, Norwegian North Sea. Journal of Structural Geology, 80, pp.99-119.

Dulanya, Z. (2017). A review of the geomorphotectonic evolution of the south Malawi rift. Journal of African Earth Sciences, 129, pp.728-738.

Dulanya, Z., Croudace, I., Reed, J.M. and Trauth, M.H. (2014). Palaeolimnological reconstruction of recent environmental change in Lake Malombe (S. Malawi) using multiple proxies. Water SA, 40(4), pp.717-728.

Dulanya, Z., Gallen, S.F., Kolawole, F., Williams, J.N., Wedmore, L.N., Biggs, J. and Fagereng, Å. (2022). Knickpoint morphotectonics of the Middle Shire River basin: Implications for the evolution of rift interaction zones. Basin Research.

Ebinger, C.J., Deino, A.L., Drake, R.E. and Tesha, A.L. (1989). Chronology of volcanism and rift basin propagation: Rungwe volcanic province, East Africa. Journal of Geophysical Research: Solid Earth, 94(B11), pp.15785-15803.

Ebinger, C.J., Jackson, J.A., Foster, A.N. and Hayward, N.J. (1999). Extensional basin geometry and the elastic lithosphere. Philosophical Transactions of the Royal Society of London. Series A: Mathematical, Physical and Engineering Sciences, 357(1753), pp.741-765.

Ebinger, C.J., Rosendahl, B.R. and Reynolds, D.J., 1987. Tectonic model of the Malawi rift, Africa. Tectonophysics, 141(1-3), pp.215-235.

Ebinger, C.J., Yemane, T., Harding, D.J., Tesfaye, S., Kelley, S. and Rex, D.C., 2000. Rift deflection, migration, and propagation: Linkage of the Ethiopian and Eastern rifts, Africa. Geological Society of America Bulletin, 112(2), pp.163-176.

Fazlikhani, H., Aagotnes, S.S., Refvem, M.A., Hamilton-Wright, J., Bell, R.E., Fossen, H., Gawthorpe, R.L., Jackson, C.A.L. and Rotevatn, A., 2021. Strain migration during multiphase extension, Stord Basin, northern North Sea rift. Basin Research, 33(2), pp.1474-1496.

Fossen, H. and Rotevatn, A., 2016. Fault linkage and relay structures in extensional settings—A review. Earth-Science Reviews, 154, pp.14-28.

Fritz, H., Abdelsalam, M., Ali, K.A., Bingen, B., Collins, A.S., Fowler, A.R., et al. (2013). Orogen styles in the East African Orogen: a review of the Neoproterozoic to Cambrian tectonic evolution. J. Afr. Earth Sci. 86, 65–106.

Garzanti, E., Bayon, G., Dinis, P., Vermeesch, P., Pastore, G., Resentini, A., Barbarano, M., Ncube, L. and Van Niekerk, H.J., 2022. The Segmented Zambezi Sedimentary System from Source to Sink: 2. Geochemistry, Clay Minerals, and Detrital Geochronology. The Journal of Geology, 130(3), pp.171-208.

Guerit, L., Yuan, X. P., Carretier, S., Bonnet, S., Rohais, S., Braun, J., & Rouby, D. (2019). Fluvial landscape evolution controlled by the sediment deposition coefficient: Estimation from experimental and natural landscapes. Geology, 47, 853–856. https://doi.org/10.1130/G46356.1

Hargrove, U.S., Hanson, R.E., Martin, M.W., Blenkinsop, T.G., Bowring, S.A., Walker, N., Munyanyiwa, H. (2003). Tectonic evolution of the Zambezi orogenic belt: geochronological, structural, and petrological constraints from northern Zimbabwe. Precambrian Res. 123 (2–4), 159–186.

Heilman, E., Kolawole, F., Atekwana, E. A., and Mayle, M. (2019). Controls of Basement Fabric on the Linkage of Rift Segments. Tectonics 38 (4), 1337–1366. doi:10.1029/2018tc005362.

Koehn, D., Aanyu, K., Haines, S., and Sachau, T. (2008). Rift nucleation, rift propagation and the creation of basement micro-plates within active rifts. Tectonophysics, 458(1–4), 105–116.

Kolawole, F. (2020). The Roles of Structural Inheritance in Regions of Induced Seismicity and Active Tectonics. PhD Dissertation, University of Oklahoma. https://hdl.handle.net/11244/324859

Kolawole, F., Atekwana, E.A., Láo-Dávila, D.A., Abdelsalam, M.G., Chindandali, P.R., Salima, J., Kalindekafe, L. (2018). Active deformation of Malawi rift's north basin Hinge zone modulated by reactivation of preexisting Precambrian Shear zone fabric. Tectonics 37 (3), 683–704.

Kolawole, F., Firkins, M.C., Al Wahaibi, T.S., Atekwana, E.A. and Soreghan, M.J. (2021a). Rift interaction zones and the stages of rift linkage in active segmented continental rift systems. Basin Research, 33(6), pp.2984-3020.

Kolawole, F., Phillips, T.B., Atekwana, E.A. and Jackson, C.A.L. (2021b). Structural inheritance controls strain distribution during early continental rifting, Rukwa Rift. Frontiers in Earth Science, p.670.

Kolawole, F., Vick, T., Atekwana, E.A., Laó-Dávila, D.A., Costa, A.G. and Carpenter, B.M. (2022). Strain localization and migration during the pulsed lateral propagation of the Shire Rift Zone, East Africa. Tectonophysics, 839, p.229499.

Konecky, B. L., Russell, J. M., Johnson, T. C., Brown, E. T., Berke, M. A., Werne, J. P., and Huang, Y. (2011). Atmospheric circulation patterns during late Pleistocene climate changes at Lake Malawi, Africa. Earth and Planetary Science Letters, 312, 318–326.

Koopmann, H., Brune, S., Franke, D. and Breuer, S., 2014. Linking rift propagation barriers to excess magmatism at volcanic rifted margins. Geology, 42(12), pp.1071-1074.

Laó-Dávila, D.A., Al-Salmi, H.S., Abdelsalam, M.G. and Atekwana, E.A., 2015. Hierarchical segmentation of the Malawi Rift: The influence of inherited lithospheric heterogeneity and kinematics in the evolution of continental rifts. Tectonics, 34(12), pp.2399-2417.

Le Pourhiet, L., Chamot-Rooke, N., Delescluse, M., May, D.A., Watremez, L. and Pubellier, M., 2018. Continental break-up of the South China Sea stalled by far-field compression. Nature Geoscience, 11(8), pp.605-609.

Lin, J. and R.S. Stein, 2004, Stress triggering in thrust and subduction earthquakes, and stress interaction between the southern San Andreas and nearby thrust and strike-slip faults, Journal of Geophysical Research, v. 109, B02303, doi:10.1029/2003JB002607.

Marrett, R. and Allmendinger, R.W., 1990. Kinematic analysis of fault-slip data. Journal of structural geology, 12(8), pp.973-986.

McClay, K. and Khalil, S., 1998. Extensional hard linkages, eastern Gulf of Suez, Egypt. Geology, 26(6), pp.563-566.

McClay, K.R., Dooley, T., Whitehouse, P. and Mills, M., 2002. 4-D evolution of rift systems: Insights from scaled physical models. AAPG bulletin, 86(6), pp.935-959.

Molnar, N.E., Cruden, A.R. and Betts, P.G., 2019. Interactions between propagating rifts and linear weaknesses in the lower crust. Geosphere, 15(5), pp.1617-1640.

Morley, C.K., 1995. Developments in the structural geology of rifts over the last decade and their impact on hydrocarbon exploration. Geological Society, London, Special Publications, 80(1), pp.1-32.

Morley, C.K., Wescott, W. A., Harper, R. M., and Cunningham, S. M. (1999). Geology and Geophysics of the Rukwa Rift. Geoscience of Rift Systems-Evolution of East Africa. AAPG Stud. Geology. 44, 91–110.

Muirhead, J.D., Wright, L.J. and Scholz, C.A., 2019. Rift evolution in regions of low magma input in East Africa. Earth and Planetary Science Letters, 506, pp.332-346.

Nelson, R. A., Patton, T. L., and Morley, C. K. (1992). Rift-segment interaction and its relation to hydrocarbon exploration in continental rift systems (1). AAPG Bulletin, 76(8), 1153–1169.

Neuharth, D., Brune, S., Glerum, A., Heine, C., and Welford, J.K. (2021). Formation of continental microplates through rift linkage: Numerical modelling and its application to the Flemish Cap and Sao Paulo Plateau. Geochemistry, Geophysics, Geosystems, 22, 1–22.

Njinju, E.A., Atekwana, E.A., Stamps, D.S., Abdelsalam, M.G., Atekwana, E.A., Mickus, K.L., Fishwick, S., Kolawole, F., Rajaonarison, T.A. and Nyalugwe, V.N. (2019a). Lithospheric structure of the Malawi Rift: Implications for magma-poor rifting processes. Tectonics, 38(11), pp.3835-3853.

Njinju, E.A., Kolawole, F., Atekwana, E.A. (2022). Coseismic static stress transfer between propagating faults promotes intra-rift faulting: Insights from the 2009 Mw 6.0 and 2014 Mw 5.2 Karonga Earthquakes, Malawi Rift. AGU Fall meeting abstract #T17a-01.

Njinju, E.A., Kolawole, F., Atekwana, E.A., Stamps, D.S., Atekwana, E.A., Abdelsalam, M. G., Mickus, K.L. (2019b). Terrestrial heat flow in the Malawi Rifted Zone, East Africa: implications for tectono-thermal inheritance in continental rift basins. J. Volcanol. Geotherm. Res. 387, 106656.

Ojo, O., Thomson, S.N., Laó-Dávila, D.A. (2022a). Neogene–Quaternary Initiation of the Southern Malawi Rift linked to reactivation of the Carboniferous–Jurassic Shire Rift. ESSOAr Preprint. https://doi.org/10.1002/essoar.10511357.1.

Ojo, O.O., Ohenhen, L.O., Kolawole, F., Johnson, S.G., Chindandali, P.R., Atekwana, E.A. and Laó-Dávila, D.A. (2022b). Under-displaced normal faults: Strain accommodation along an early-stage rift-bounding fault in the Southern Malawi Rift. Frontiers in Earth Science, 10.

Palamuleni, L.G., Ndomba, P.M. and Annegarn, H.J., 2011. Evaluating land cover change and its impact on hydrological regime in Upper Shire River catchment, Malawi. Regional Environmental Change, 11(4), pp.845-855.

Patton, T.L., Moustafa, A.R., Nelson, R.A. and Abdine, S.A., 1994. Tectonic evolution and structural setting of the Suez rift: chapter 1: Part I. Type basin: Gulf of Suez.

Pfaffling, A., Monstad, S., Groom, R.W. and Rudd, J., 2009. Airborne-EM hydrocarbon mapping in Mozambique. ASEG Extended Abstracts, 2009(1), pp.1-6.

Price, T., 1966. Shire, Shirwa, and Nyasa. The Society of Malawi Journal, pp.15-19.

Ragon, T., Nutz, A., Schuster, M., Ghienne, J. F., Ruffet, G., and Rubino, J. L. (2019). Evolution of the Northern Turkana Depression (East African Rift System, Kenya) during the Cenozoic Rifting: New Insights from the Ekitale Basin (28-25.5 Ma). Geol. J. 54 (6), 3468–3488. doi:10.1002/gj.3339.

Rosendahl, B.R., 1987. Architecture of continental rifts with special reference to East Africa. Annual Review of Earth and Planetary Sciences, 15(1), pp.445-503.

Rosendahl, B.R., Reynolds, D.J., Lorber, P.M., Burgess, C.F., McGill, J., Scott, D., Lambiase, J.J. and Derksen, S.J., 1986. Structural expressions of rifting: lessons from Lake Tanganyika, Africa. Geological Society, London, Special Publications, 25(1), pp.29-43.

Russell, J.M., Cohen, A.S., Johnson, T.C. and Scholz, C.A., 2012. Scientific drilling in the East African Rift Lakes: A strategic planning workshop. Scientific Drilling, 14, pp.49-54.

Rotevatn, A., Kristensen, T., Ksienzyk, A., Wemmer, K., Henstra, G., Midtkandal, I., Grundvåg, S.A., Andresen, A., 2018. Structural inheritance and rapid rift-length establishment in a multiphase rift: the East Greenland rift system and its Caledonian orogenic ancestry. Tectonics 37, 1858–1875.

Ryan, W. B. F., S.M. Carbotte, J. Coplan, S. O'Hara, A. Melkonian, R. Arko, R.A. Weissel, V. Ferrini, A. Goodwillie, F. Nitsche, J. Bonczkowski, and R. Zemsky (2009), Global Multi-Resolution Topography (GMRT) synthesis data set, Geochem. Geophys. Geosyst., 10, Q03014.

Sachau, T., Koehn, D., Stamps, D.S. and Lindenfeld, M., 2016. Fault kinematics and stress fields in the Rwenzori Mountains, Uganda. International Journal of Earth Sciences, 105, pp.1729-1740.

Sander, S. and Rosendahl, B.R., 1989. The geometry of rifting in Lake Tanganyika, east Africa. Journal of African Earth Sciences (and the Middle East), 8(2-4), pp.323-354.

Saria, E., Calais, E., Stamps, D.S., Delvaux, D. and Hartnady, C.J.H., 2014. Present-day kinematics of the East African Rift. Journal of Geophysical Research: Solid Earth, 119(4), pp.3584-3600.

Schmid, T.C., Brune, S., Glerum, A. and Schreurs, G., 2023. Tectonic interactions during rift linkage: Insights from analog and numerical experiments. EGU Solid Earth, 14, 389–407.

Scholz, C. A., Cohen, A. S., Johnson, T. C., King, J., Talbot, M. R., and Brown, E. T. (2011). Scientific drilling in the Great Rift Valley: The 2005 Lake Malawi Scientific Drilling Project—An overview of the past 145,000 years of climate variability in Southern Hemisphere East Africa. Palaeogeography, Palaeoclimatology, Palaeoecology, 303(1–4), 3–19.

Scholz, C.A. and Rosendahl, B.R., 1988. Low lake stands in Lakes Malawi and Tanganyika, East Africa, delineated with multifold seismic data. Science, 240(4859), pp.1645-1648.

Scholz, C.A., Shillington, D.J., Wright, L.J., Accardo, N., Gaherty, J.B., Chindandali, P. (2020). Intrarift fault fabric, segmentation, and basin evolution of the Lake Malawi (Nyasa) Rift, East Africa. Geosphere 16 (5), 1293–1311.

Specht, T. D., and Rosendahl, B. R. (1989). Architecture of the Lake Malawi Rift, East Africa. J. Afr. Earth Sci. 8 (2–4), 355–382. doi:10.1016/s0899-5362(89). 80032-6.

Stamps, D. S., Calais, E., Saria, E., Hartnady, C., Nocquet, J. M., Ebinger, C. J., & Fernandes, R. M. (2008). A kinematic model for the East African Rift. Geophysical Research Letters, 35, L05304. https://doi.org/10.1029/2007GL032781.

Stamps, D.S., Saria, E., Kreemer, C. (2018). A geodetic strain rate model for the East African Rift system. Sci. Rep. 8 (1), 1–8.

Stevens, V.L., Sloan, R.A., Chindandali, P.R., Wedmore, L.N., Salomon, G.W., Muir, R.A., 2021. The entire crust can be seismogenic: evidence from Southern Malawi. Tectonics 40(6). https://doi.org/10.1029/2020TC006654 e2020TC006654.

Sun, M., Gao, S.S., Liu, K.H., Mickus, K., Fu, X. and Yu, Y., 2021. Receiver function investigation of crustal structure in the Malawi and Luangwa rift zones and adjacent areas. Gondwana Research, 89, pp.168-176.

Thomas, R.J., Fullgraf, T., Macey, P.H., Boger, S.D., Hölttä, P., Lach, P., Le Roux, P., Dombola, K. and Zammit, C. (2022). The Mesoproterozoic Nampula Subdomain in southern Malawi: Completing the story from Mozambique. Journal of African Earth Sciences, 196, p.104667.

Toda, S., R. S. Stein, K. Richards-Dinger and S. Bozkurt, 2005, Forecasting the evolution of seismicity in southern California: Animations built on earthquake stress transfer, Journal of Geophysical Research, v. 110, B05S16, doi:10.1029/2004JB003415.

Wedmore, L.N., Williams, J.N., Biggs, J., Fagereng, Å., Mphepo, F., Dulanya, Z., Willoughby, J., Mdala, H., Adams, B., 2020a. Structural inheritance and border fault reactivation during active early-stage rifting along the Thyolo fault, Malawi. J. Struct. Geol. 139, 104097.

Wedmore, L.N.J., Biggs, J., Williams, J.N., Fagereng, Å., Dulanya, Z., Mphepo, F. and Mdala, H., 2020b. Active fault scarps in southern Malawi and their implications for the distribution of strain in incipient continental rifts. Tectonics, 39(3), p.e2019TC005834.

Williams, J.N., Fagereng, Å., Wedmore, L.N., Biggs, J., Mphepo, F., Dulanya, Z., Mdala, H., Blenkinsop, T. (2019). How do variably striking faults reactivate during rifting? Insights from southern Malawi. Geochem. Geophys. Geosyst. 20 (7), 3588–3607.

Williams, J.N., Wedmore, L.N., Scholz, C.A., Kolawole, F., Wright, L.J., Shillington, D.J., Fagereng, Å., Biggs, J., Mdala, H., Dulanya, Z. and Mphepo, F., 2022. The Malawi active fault database: An onshore-offshore database for regional assessment of seismic hazard and tectonic evolution. Geochemistry, Geophysics, Geosystems, 23(5), p.e2022GC010425.

Wilson, D.S., 1990. Kinematics of overlapping rift propagation with cyclic rift failure. Earth and Planetary Science Letters, 96(3-4), pp.384-392.

Wolf, L., Huismans, R.S., Wolf, S.G., Rouby, D. and May, D.A., 2022. Evolution of rift architecture and fault linkage during continental rifting: Investigating the effects of tectonics and surface processes using lithosphere-scale 3D coupled numerical models. Journal of Geophysical Research: Solid Earth, p.e2022JB024687.

Van Wijk, J.W. and Blackman, D.K., 2005. Dynamics of continental rift propagation: the end-member modes. Earth and Planetary Science Letters, 229(3-4), pp.247-258.

Yuan, X. P., Braun, J., Guerit, L., Simon, B., Bovy, B., Rouby, D., et al. (2019). Linking continental erosion to marine sediment transport and deposition: A new implicit and O(N) method for inverse analysis. Earth and Planetary Science Letters, 524, 115728. https://doi.org/10.1016/j.epsl.2019.115728

Yuan, X. P., Braun, J., Guerit, L., Rouby, D., & Cordonnier, G. (2019). A new efficient method to solve the stream power law model taking into account sediment deposition. Journal of Geophysical Research: Earth Surface, 124, 1346–1365. https://doi.org/10.1029/2018JF004867

Zwaan, F., Chenin, P., Erratt, D., Manatschal, G. and Schreurs, G., 2022. Competition between 3D structural inheritance and kinematics during rifting: Insights from analogue models. Basin research, 34(2), pp.824-854.

Zwaan, F. and Schreurs, G., 2017. How oblique extension and structural inheritance influence rift segment interaction: Insights from 4D analog models. Interpretation, 5(1), pp.SD119-SD138.

Figures

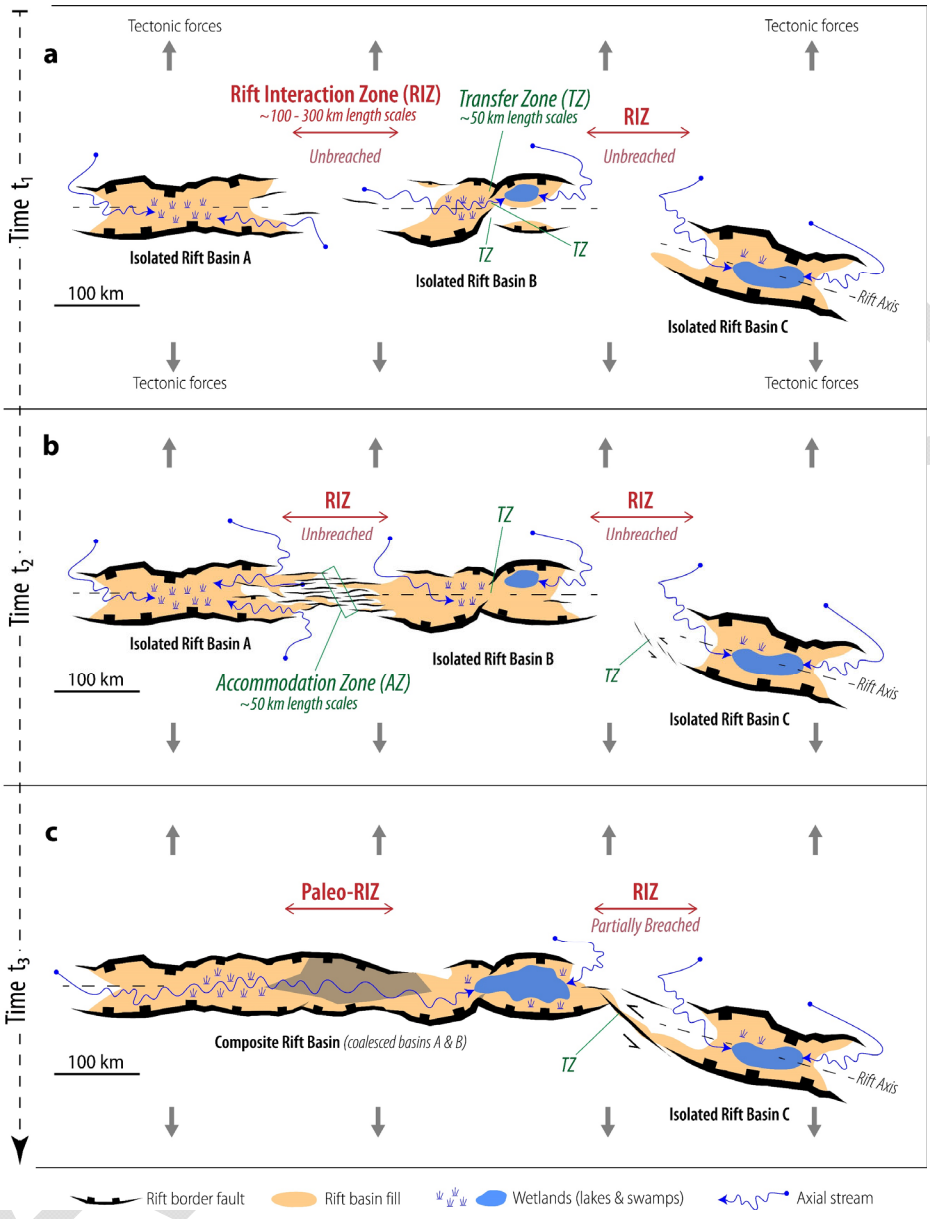

Figure 1. Cartoon illustrating the evolution of zones of rift segment interaction along narrow continental rift systems during **(a)** the initial nucleation of isolated rift basins, to **(b)** subsequent lateral propagation and interaction, and **(c)** linkage and coalescence of the basins. Prior to linkage and coalescence, the broad region of interaction between the rifts (~100 – 300-km length scales) are referred to as a 'rift interaction zones (RIZ)' (Nelson et al., 1992; Kolawole et al., 2021a). RIZs commonly host transfer and accommodation zones and their associated structures that localize and transfer strain across the RIZs (Bosworth, 1985; Ebinger et al., 1987; Morley et al., 1990; Nelson et al., 1992; Morley, 1995; Faulds and Varga, 1998). RIZ geometries can be defined by the relative trend and border fault dip polarity of the interacting rift basins (after Morley et al., 1990) such as Tip-to-Tip Collinear (e.g., between Rift Basins A and B in Panels a & b) and Underlapping oblique convergent (e.g., between Rift Basins B and C in Panels a & b) (Kolawole et al., 2021a).

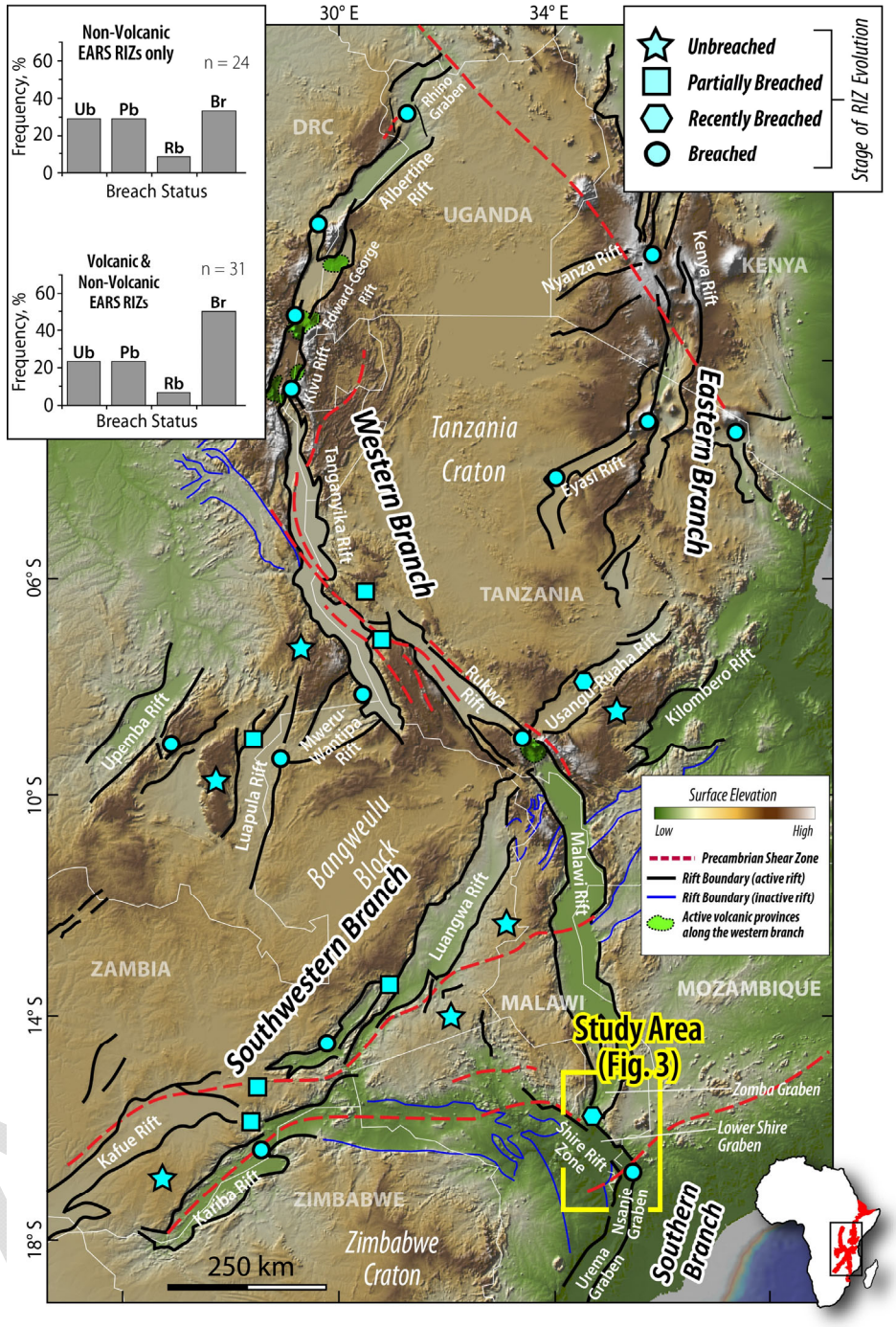

Figure 2. Topographic relief map of the East African Rift System (EARS; Source: Ryan etal., 2009), showing the magma-rich eastern branch, and magma-poor western, southwestern, and southern branches. The symbols represent the stage of evolution of its rift interaction zones (RIZ), inferred from spatial extents of fault connectivity and topographic, and drainage morphology of the RIZs (Kolawole et al., 2021a). Histograms show the distribution of RIZ evolution stages along the rift system (from Kolawole et al., 2021a), and UB, PB, RP and Br are short for Unbreached, Partially breached, Recently breached, and breached respectively. Note that the EARS is defined by the active rift segments (black lines). *Bottom right inset:* Map of Africa showing the East African Rift System (red polygons) and region covered by the relief map (black rectangle).

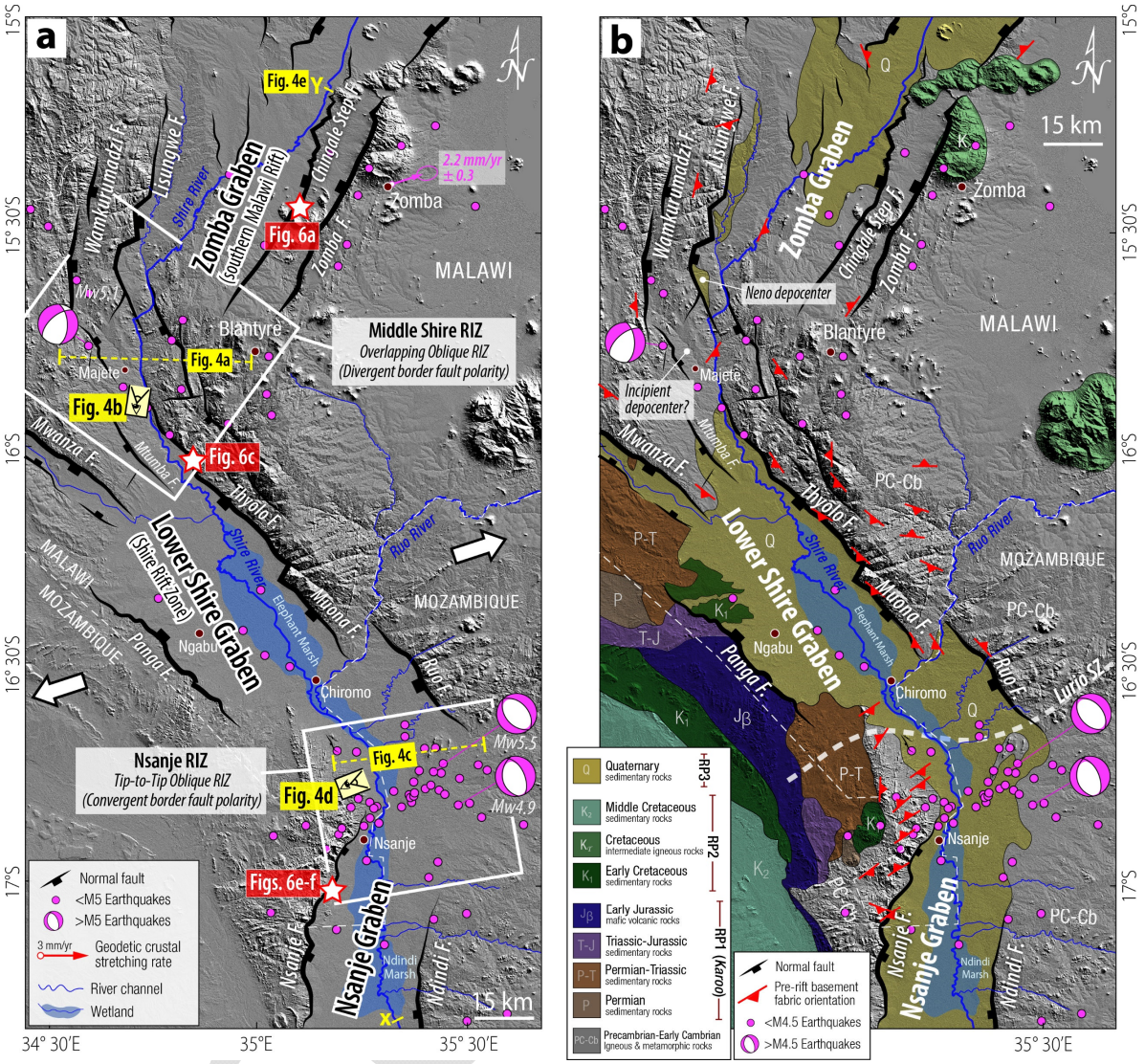

Figure 3. a. Topographic relief map of southern Malawi and central Mozambique, showing the contiguous Zomba Graben (Malawi Rift), the Lower Shire Graben (Shire Rift Zone), and Nsanje Graben, and their intervening Middle Shire and Nsanje Rift Interaction Zones (RIZ). The main axial stream in the region, the Shire River and its tributaries, drains all the three rift basins and flows further south into the Indian Ocean. Fault segments are surface-breaking active faults from Williams et al. (2022) and Kolawole et al. (2022). Earthquakes and focal mechanisms are from the US Geological Survey earthquake catalog, Global CMT catalog, and Stevens et al. (2021) covering 1966 to 2020. Geodetic crustal stretching azimuth is from Stamps et al. (2008, 2018). Basement metamorphic fabric orientations are from Williams et al. (2019), Kolawole et al. (2022), Thomas et al. (2022), and field observations in this study. **b.** Geologic map of the southern Malawi region and western Mozambique (modified after Choubert et al., 1988; Kolawole et al., 2022).

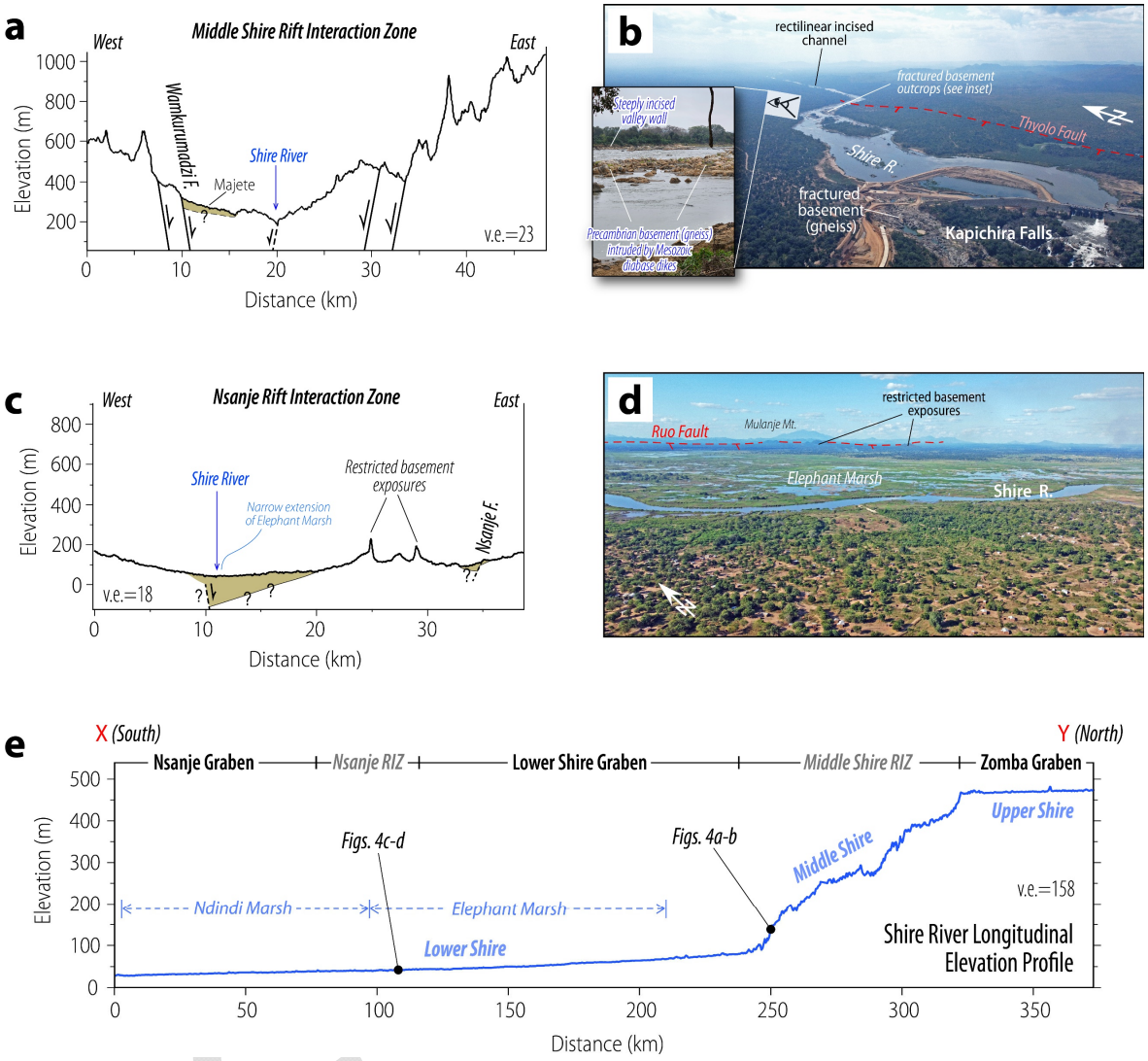

Figure 4. a – d. Topographic relief profiles (panels a & c; 30-m resolution Shuttle Radar Topography Mission data) and field photographs (panels b & d) showing rift morphology across the Middle Shire RIZ (a – b) and Nsanje RIZ (c – d). Sediment depocenters color coded in yellow. **e.** Longitudinal topographic relief profile of the Shire River (see Figure 3a for the start and end of the profile labelled as x and y).

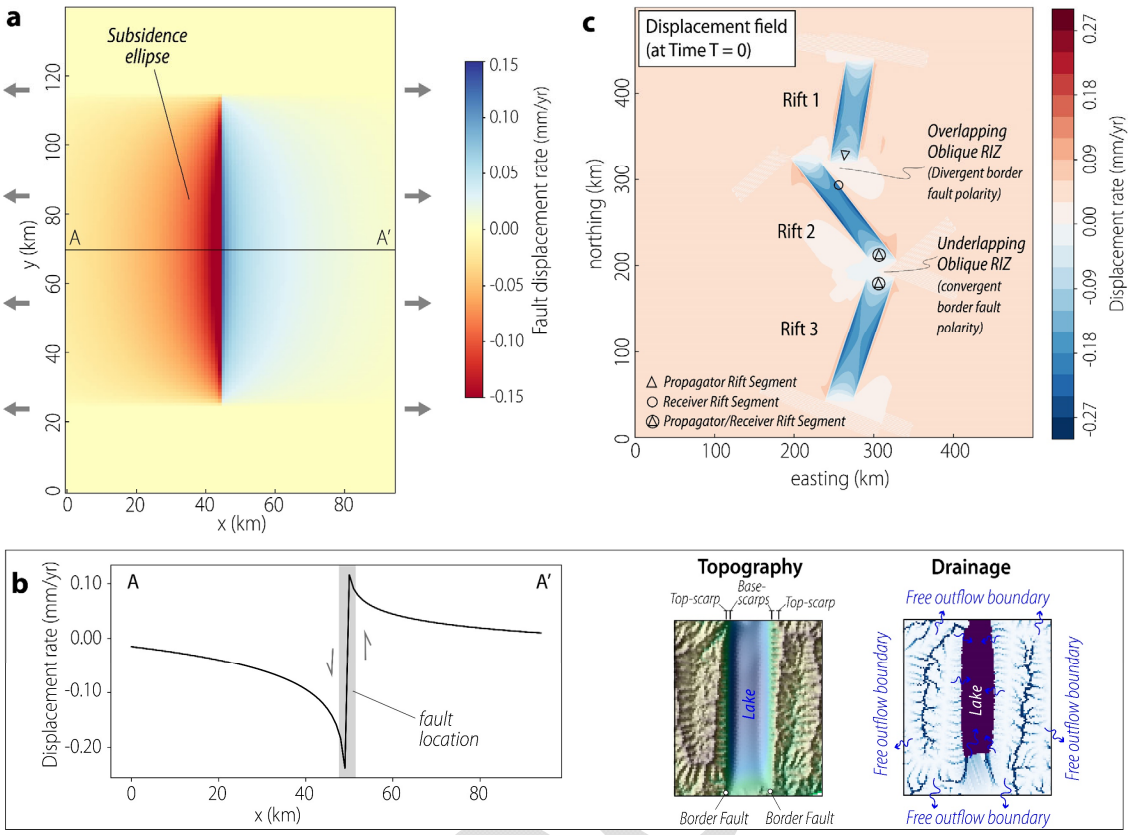

Figure 5. Model setup to simulate landscape evolution across two contiguous rift interaction zones with geometries similar to those of the Middle Shire and Nsanje rift interaction zones. **a - b.** Fault segment uplift field with hanging wall subsidence and footwall uplift. Inset maps in panel b shows the resulting topography and drainage for a graben configuration. **c.** Initial displacement field applied in the model to estimate the fault development and rift evolution.

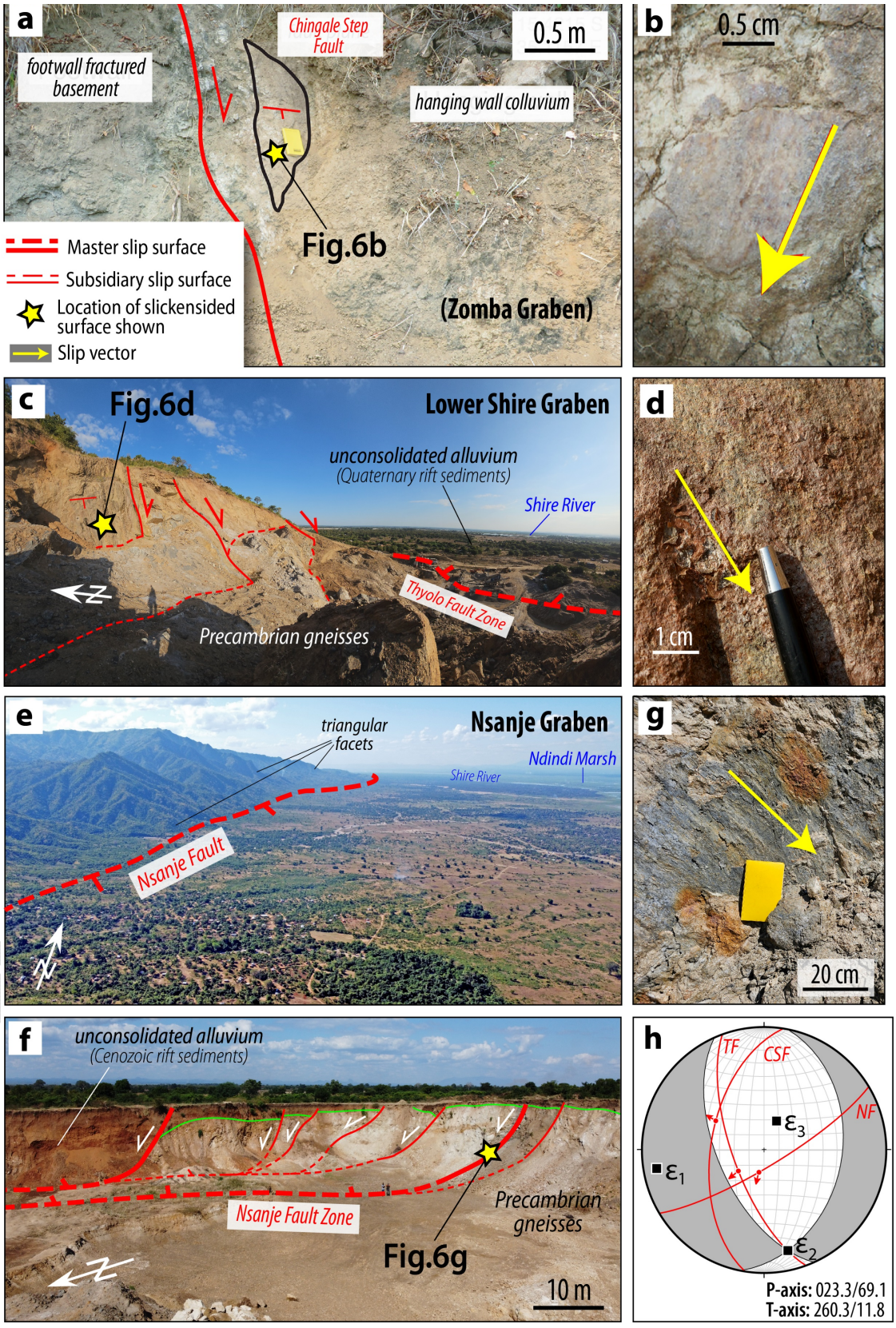
a
Chingale Step Fault
0.5 m
footwall fractured basement
hanging wall colluvium
Fig.6b
(Zomba Graben)
Master slip surface
Subsidiary slip surface
Location of slickensided surface shown
Slip vector
b
0.5 cm
c
Fig.6d
Lower Shire Graben
unconsolidated alluvium
(Quaternary rift sediments)
Shire River
Thyolo Fault Zone
Precambrian gneisses
d
1 cm
e
triangular facets
Nsanje Graben
Ndindi Marsh
Shire River
Nsanje Fault
g
20 cm
f
unconsolidated alluvium
(Cenozoic rift sediments)
Nsanje Fault Zone
Precambrian gneisses
Fig.6g
10 m
h
TF
CSF
NF
ε3
ε1
ε2
P-axis: 023.3/69.1
T-axis: 260.3/11.8

Figure 6. a – f. Field photographs showing slip surfaces along the Chingale Step Fault, Zomba Graben (panels a – b; photographs from Wedmore et al., 2020b), Thyolo Fault, Lower Shire Graben (panels c – d), and the Nsanje Fault, Nsanje Graben (panels e – g). See Figure 3a for the location of the photos and look-direction of the landscape shots. **h.** Kinematic Tensor solution produced from the combined geological slip vectors measured along the three faults (i.e., Figures 7b, d, and g; see *Methods* section). ε_1, ε_2, and ε_3 represent the principal strain axes 1 (extension), 2 (intermediate), and 3 (shortening) respectively. The solution shows a predominantly normal faulting regime, although with a minor strike-slip component.

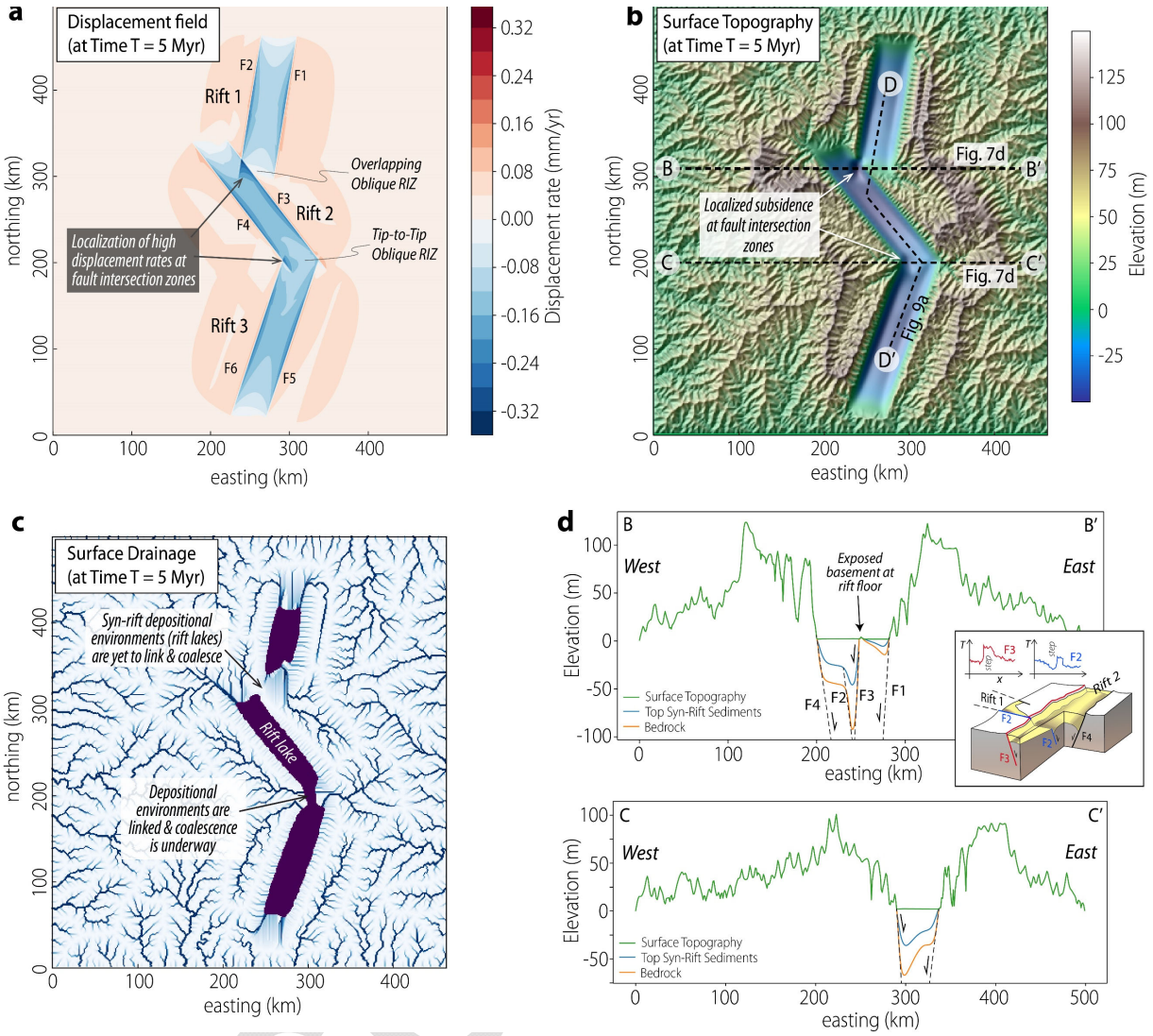

Figure 7. a. Displacement field, **b.** modeled topography, and **c.** drainage map at 5 Myr, showing the large-scale fault structure and surface morphology of the laterally propagating and interacting rift tips. **d.** Cross-sections A-A' across the overlapping oblique rift interaction zone (RIZ), and B-B' across the tip-to-tip oblique RIZ. Note that the tip-to-tip oblique RIZ was initially an underlapping oblique RIZ at T=0 Myr (Figure 5c). *7d inset:* 3-dimensional (3D) schematic showing the large-scale structure of antithetically linked faults as seen in the model results (Figs. 7a-b) and idealized throw-distance (T-x) plots inspired by the model results and natural examples (e.g., Duffy et al., 2015).

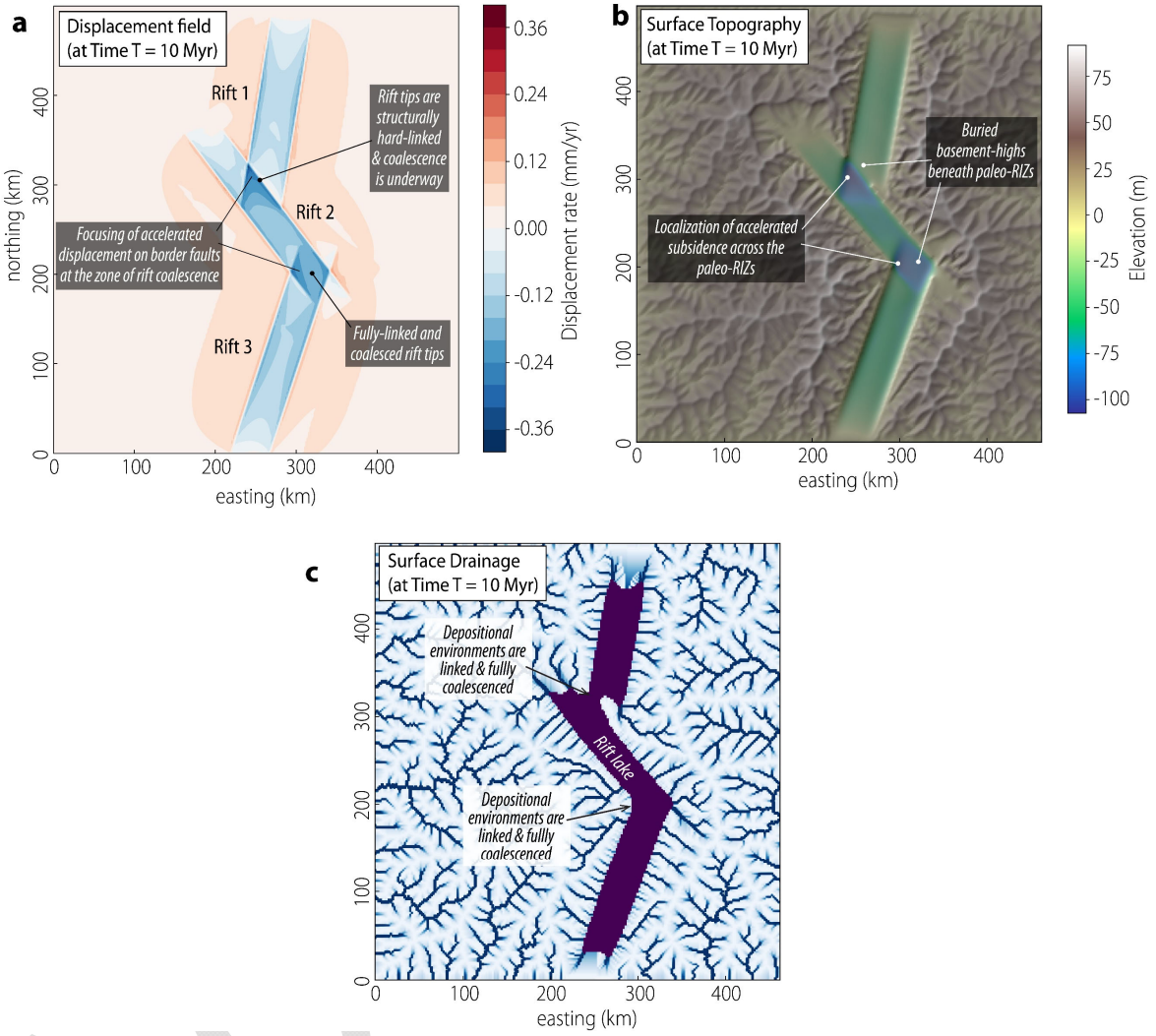

Figure 8. a. Displacement field, **b.** modeled topography, and **c.** drainage map at 10 Myr showing complete rift coalescence across the tip-to-tip RIZ and established hard-linkage with ongoing coalescence across the overlapping RIZ. Interestingly, the results also highlight that once rift linkage is established, rift coalescence is accompanied by the focusing of accelerated fault displacement and basin subsidence across the deforming RIZs.

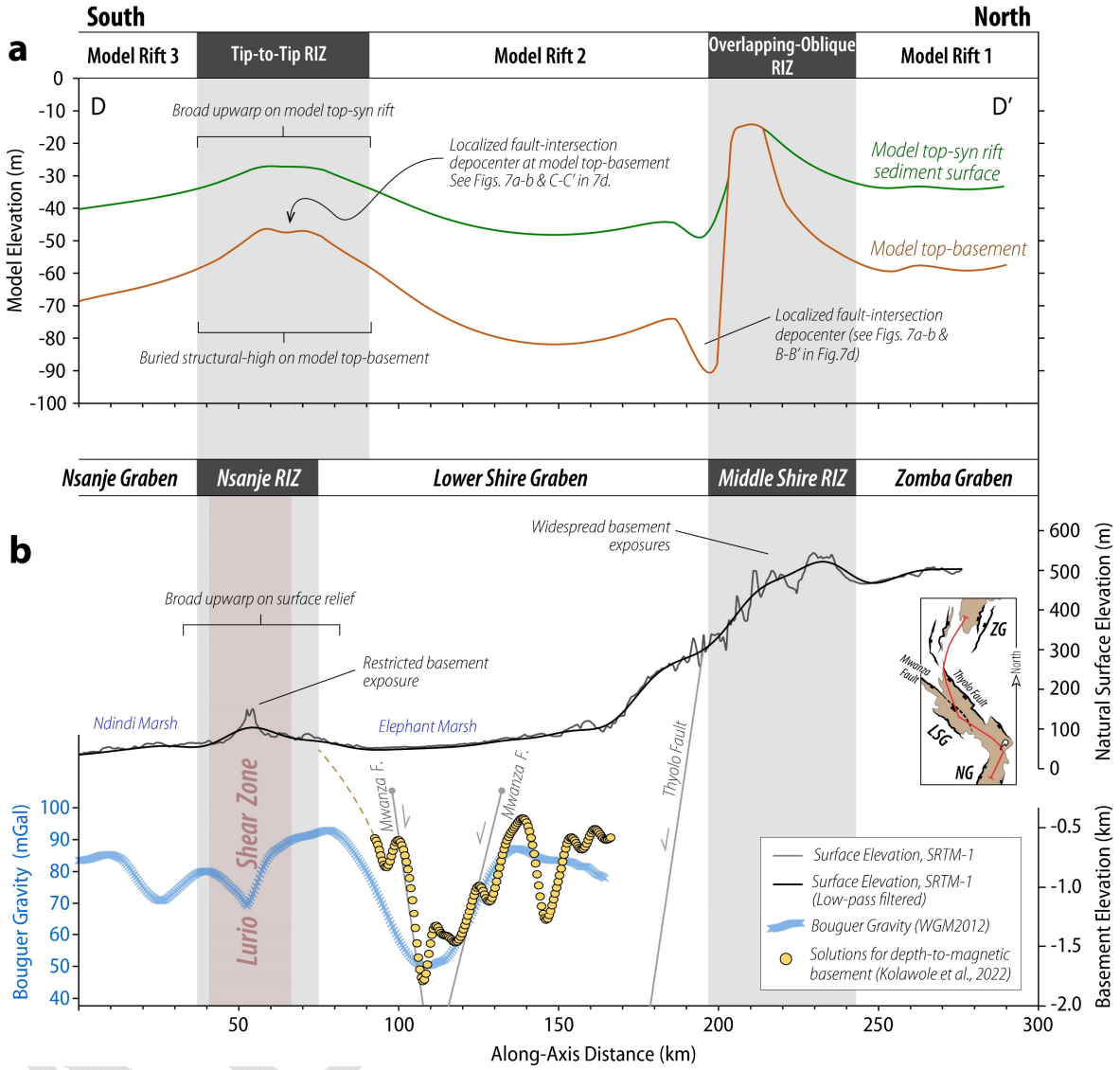

Figure 9. a. Plot comparing the along-axis model surface relief, model top-synrift surface relief, and model top-basement relief (at 5 Myr time step) with the natural along-axis variation in surface topographic relief in the studied rifts. See transect for profile D-D' in Figure 9b (modeled topography) and Figure S1 (natural topography). **b.** Along-axis plot of natural surface relief along the rifts, Bouguer gravity anomaly, and variation of basement elevation (transect in inset map; NG- Nsanje Graben, LSG- Lower Shire Graben, ZG- Zomba Graben). The natural topography data is from 30 m-resolution Shuttle Radar Topography Mission (SRTM), Bouguer gravity data from World Gravity global model, WGM2012 (Figure S3; Bonvalot et al., 2012), and basement depths calculated from aeromagnetic grid (Kolawole et al., 2022).

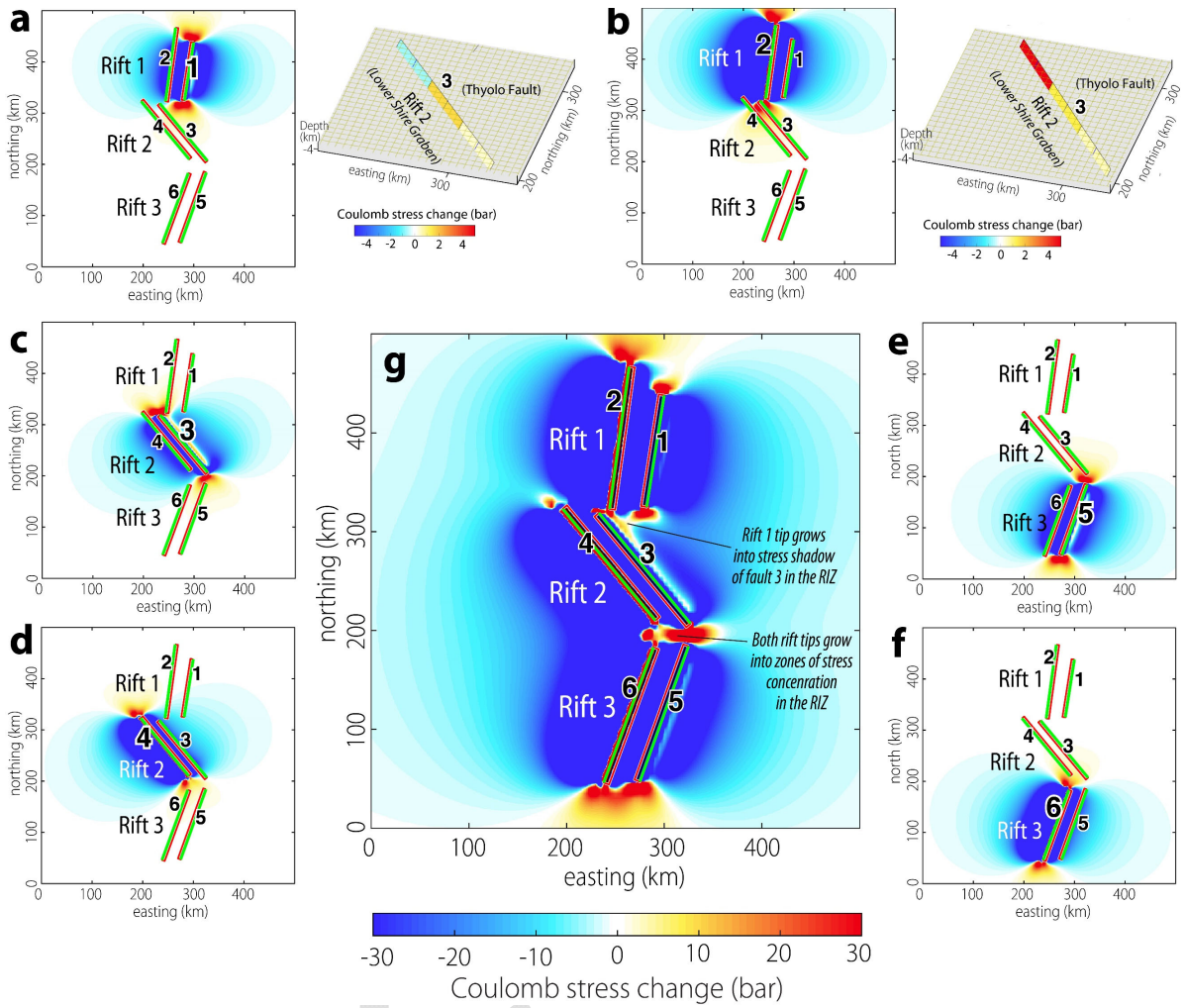

Figure 10. a – f. Model results of predicted static Coulomb stress change distribution for instances of slip on each of the border faults (as source fault, enlarged fault number) of the model rift basins, maintaining the same input rift geometries and model parameters used for the Landscape evolution model. We assume a coefficient of friction of 0.55, appropriate for the southern Malawi region (Williams et al., 2019), and fault rupture depth of 5 km. In each model, the entire border fault length ruptures in a single event. Note that numbers 1 to 6 represent fault identifiers. 3-D views in panels a and b show Coulomb stress changes on fault 3 with slip on source fault 1 (a) and fault 2 (b), illustrating the difference effects of these two fault slip events on the stress field of fault 3 in the RIZ. **g.** Static Coulomb stress change distribution for the same model domain as shown in a -f, but in which all the border faults act as source faults. Coulomb stress change is calculated for N-S striking faults with a potential rake of -90 (normal dip-slip). Altogether, the models show that in overlapping RIZs, the propagating rift tip grows into a stress relaxation zone, which contrasts tip-to-tip RIZs where propagating rift tips grow into a compounding stress concentration zone.